jntes

JOURNAL OF NEW TECHNOLOGIES IN ENVIRONMENTAL SCIENCE

2

2023

No. 2 Vol. 7 ISSN 2544-7017 www.jntes.tu.kielce.pl Kielce University of Technology

CONTENTS

www.jntes.tu.kielce.pl
jntes@tu.kielce.pl

The quarterly printed issues of Journal of New Technologies in Environmental Science are their original versions. The Journal published by the Kielce University of Technology.

ISSN 2544-7017

Doi: 10.53412

Natalia KRAWCZYK[1], Luiza DĘBSKA[1]
Stanislav HONUS[2], Marta ZEGAREK[1]
Mateusz KINIORSKI[1], Łukasz J. ORMAN[1]
[1] *Faculty of Environmental Engineering, Geodesy and Renewable Energy, Kielce University of Technology, Kielce, Poland*
[2] *Faculty of Mechanical Engineering, VSB – Technical University of Ostrava, Ostrava-Poruba, Czech Republic*
Corresponding author: orman@tu.kielce.pl

Doi: 10.53412/jntes-2023-2-1

THERMAL COMFORT TESTING IN THE SMART SUSTAINABLE BUILDING

Abstract: *Today, more and more buildings are being built based on the idea of sustainable development. This mainly concerns the creation of such microclimate conditions in the rooms that a person feels comfortable inside. Therefore, the article presents tests of thermal comfort for three teaching rooms in an intelligent building. The research was carried out using two methods, a microclimate meter measurements and questionnaires. The survey provided research results on thermal sensation vote, thermal preference vote and humidity assessment. Moreover, the results of Predicted Percentage of Dissatisfied and Predicted Mean Vote were presented in the paper. Students between the age of 21 and 25 and one female in her 30s participated in the survey. Through the results of the questionnaires and the microclimate meter, significant differences were shown between the Fanger model and the questionnaires in terms of PMV and PPD.*

Keywords: *sustainable development, microclimate conditions, thermal comfort, classrooms, Fanger model*

Introduction

A person spends most of his/her life in closed rooms. Therefore, more and more attention is paid to the optimal conditions of the internal environment. At the same time, intelligent buildings are being created more and more often, in which it is possible to provide an appropriate microclimate and appropriate thermal comfort to its users. These buildings are made with care for the natural environment and are made of ecological materials. Thanks to the production of energy and heat using renewable energy sources (solar and photovoltaic panels, heat pumps, etc.), intelligent buildings are self-sufficient. The parameters and changes in the production of heat, energy and lighting changes in the building are controlled with the use of the Building Management System (BMS), which is the main indicator of sustainable construction. Thermal comfort determines that we are comfortable under given climatic conditions. The term indoor microclimate should be understood as a set of factors determining the well-being of a person inside the room. The feeling of thermal comfort is influenced by variable parameters, including: air temperature, average radiation temperature, air humidity, thermal insulation of clothing, air flow velocity and physical activity. It is essential to guarantee optimal climate conditions in existing and modern buildings, where people will not be too warm or too cold. People want to live in a comfortable environment. Therefore, the climate of the room should be adjusted so that it suits the majority. If you do not have the right climate, your body will be affected. The human body has various biological features. This results in different sensations when being in the same conditions. Our body's temperature regulation system is responsible for balancing our body. Unhealthy climate conditions can contribute to a person's fatigue. Also, they can affect health, productivity, and mood. To guarantee

thermal comfort, residents need to make sure their air conditioning is adequate. The sense of thermal comfort also affects our productivity. This is why thermal comfort is an important aspect.

In order to determine the appropriate thermal comfort, it is necessary to take into account as many components as possible that influence the thermal sensations experienced by humans. The thermal comfort model was developed by O. Fanger in the 1970s and was used to create the methodology set out in the standards [1, 2].

According to the use of his own research and literature, Fanger [3] developed a concept of using two indices: PMV – Predicted Mean Vote and PPD – Predicted Percentage of Dissatisfied. The thermal comfort diagram is defined as a function of the mean ambient radiant temperature, physical activity, air temperature, clothing insulation, and humidity. The PMV index is an assessment of the thermal impressions of room users on a seven-point scale, where "-3" means "cold", "+3" hot, and the desired range is around zero. Currently, more and more researchers are conducting research on thermal comfort. Becker and Paciuk [4] performed testing in buildings, where the authors surveyed 189 apartments in winter and 205 in summer. Their findings showed that Predicted Mean Vote in summer was below zero, while the opposite was true in winter. They found that the survey results differed from the calculated PMV. Tests of Broday et al. [5] dealt with 25 climate-controlled buildings. They documented that the standard [1] for PMV values does not reflect the real feelings of the respondents. In turn, other authors [6, 7] have made similar observations. In addition, the authors also noted inconsistency between actual observations and PMV index calculations. An interesting study on warmth comfort was conducted by Bartal et al. [8]. In this paper they gave out the analysis of the thermal equilibrium of the individual body and the heat deficit due to perspiration. Attention was also given to how the temperature comfort graph evolves for lightly dressed people at different activity levels. Homoda et al. [9] analysed the indices related to thermal comfort, namely PMV and PPD. In their study, they showed that thermal sensation is affected to the biggest extent by temperature and relative air humidity. Krawczyk and Krakowiak [10] analysed thermal comfort in two educational buildings, modern and traditional. There were 24 participants in the study – performed in June. In the article you can notice the variance between the scores of the PMV and the scores of the surveys. The consideration showed that answerers would rather to have higher relative humidity indoors. In Poland, research on thermal comfort is also done [11, 12]. The authors [13] showed in their work the dissimilarities between the real feelings from the polls and the PMV results for 39 people. The differences between the results were significantly influenced by low light levels, high carbon dioxide concentration and high noise levels. Zhang et al. [14] modelled thermal comfort phenomena for intelligent buildings. The authors proved that nonlinear models performed better than linear models. In his article, Jindal [15] conducted a study on 130 school-age students to investigate the thermal environment and their thermal perception. He found that students felt best in the operational range of 15.5°C to 33.7°C. Contrastingly, the authors [16, 17] oversaw research on thermal comfort in hospital buildings. The Thermal Sensation Vote values were higher than the calculated PMV values. Furthermore, Dębska and Krakowiak [18] conducted research in a sustainable building, in which it was shown that the tested room meets the thermal acceptance of people, meeting the criteria of sustainable construction.

The idea of this paper is to provide data on thermal comfort conditions in the intelligent building. As stated by the presented literature review, it was noticed that the results obtained with the Fanger model are not identical with the actual experimental results. This study focuses mainly on the feelings of the respondents in three classrooms and their sensations regarding the climatic conditions. Such studies in intelligent buildings are not common these days due to the fact that such buildings are still rare, besides online education at some locations makes such tests impossible. Thus, the present paper would expend the knowledge on the analysed subject.

Materials and Methods

At the Kielce University of Technology in Poland, the experimentation was managed in October and early November at the "Energis" building of the Faculty of Environmental, Geomatic and Energy Engineering (Fig. 1).

FIGURE 1. *Photo of "Energis" from the Northern side – main entrance to the building*

The Energis smart building has mechanical ventilation. The ventilation was not used during the study. The building has photovoltaic cells, heat pumps and solar collectors. The rooms under study are located on the Western side. Thermal insulation of the building is generally fine. It was tested with infrared camera. Figure 2 shows the thermograph of the Eastern part of the Energis building, where windows seem to be a source of increased thermal losses.

FIGURE 2a. *Photo of "Energis" from the Eastern side*

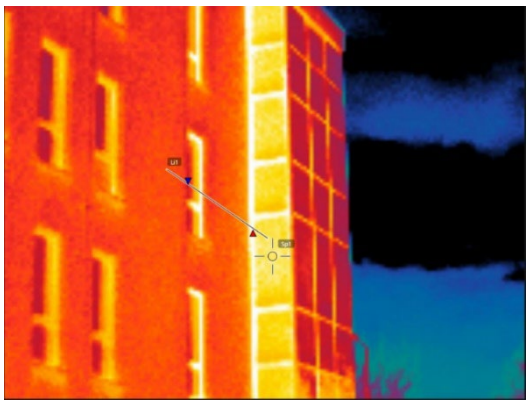

FIGURE 2b. *Thermographic image of the Eastern side of "Energis"*

Thermal comfort tests were carried out in three classrooms using two methods. The first method was performed with a Testo 400 microclimate meter. The measurements during the study included air speed and temperature, light intensity, relative humidity, black sphere temperature and CO_2 concentration. The properties were read from a microclimate meter 15 minutes after the test results had stabilised. During the measurements, people in the rooms filled in an anonymous questionnaire (which can be considered as the second method). The survey concerned thermal sensations of the microclimate. Additionally, the questionnaire was about the type of clothing the interviewees were wearing. From this, the level of heating resistance of the office chair (0.1 clo) and the insulation performance of the clothing were determined. The thermal resistance of the study group ranged from 0.59 clo to 0.63 clo. Metrics with data on age, height, gender, and weight were at the end of the survey. Thanks to this, the Body Mass Index (BMI) was calculated, which was used for comparison with Thermal Sensation Vote (TSV). The Figure 3 shows a diagram of changes in air temperature, humidity and CO_2 in one room.

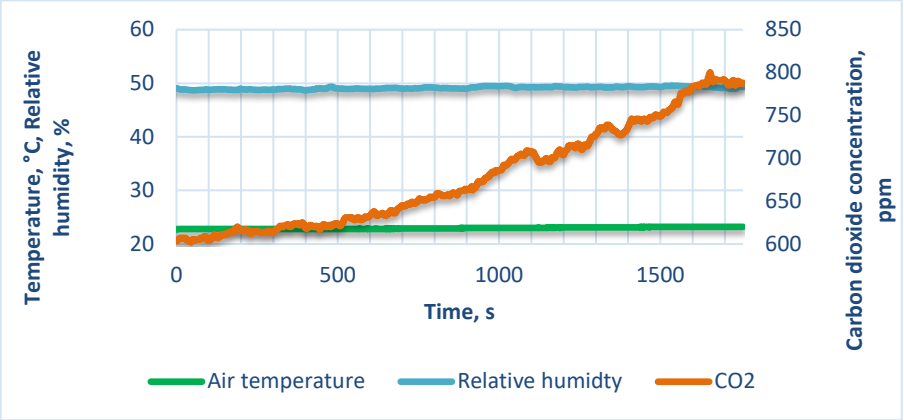

FIGURE 3. *Graph of changes in air temperature, air humidity and carbon dioxide*

Figure 3 shows the changes in the concentration of carbon dioxide, relative humidity and air temperature during the test. From the graph, you can see that the temperature and relative humidity remained almost the same throughout the study. At the beginning of the study, the temperature was 22.7°C, and at the end of the study: 23.2°C. Relative humidity at the beginning of the test was 49.06%, while at the end of the test: 49.29%. It is worth noting the greatest differences in the concentration of carbon dioxide. It was 603 ppm at the beginning and 788 ppm at the end.

Surveys were taken in the autumn season. Thirty-seven people responded to the survey, comprising 13 females and 24 males between the ages of 21 and 25 and one woman in her 30s. Volunteers were asked about the environments in the room. The survey scores were paralleled with the results from the specialized equipment of the Testo 400 microclimate meter. Figure 4 shows the response frequency (%) regarding the thermal sensation vote.

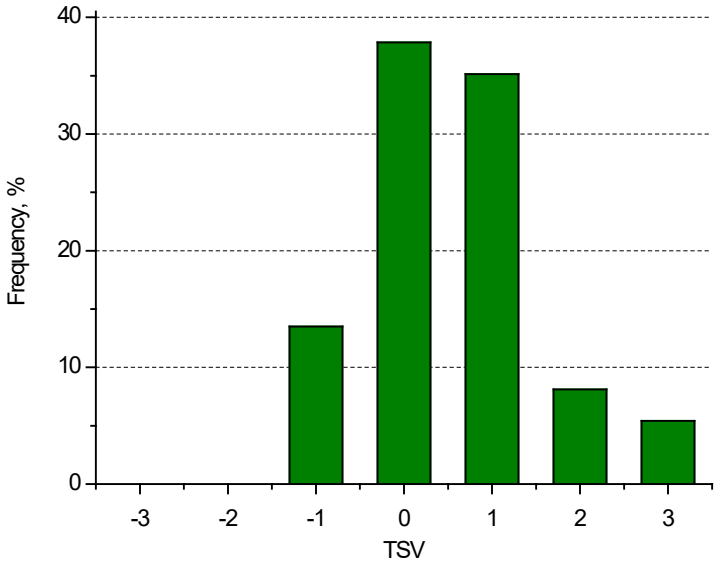

FIGURE 4. *TSV on the basis of surveys*

TSV (Thermal Sensation Vote) are actual thermal sensations that were determined using an anonymous survey. In the questionnaire, TSV was determined by each person using a seven-point scale: "-3" – too cold, "-2" – too cool, "-1" – pleasantly cool, "0" – comfortable, "1" – pleasantly warm, "2" – too warm, "3" – too hot. It can be seen from the chart that the thermal conditions in the three rooms are comfortable for 37.84% of the respondents. So 14 participants out of 37 picked this response. During the measurements, ventilation was turned off. The air was exchanged through tilted windows. The second most frequently given answer by the respondents was the pleasantly warm option, which amounted to

35.14% (13 people). Five people were pleasantly cool, which is 13.51%. Three respondents chose the answer too warm (8.11%), and two people too hot (5.41%). It should be noted that the proportion of people who chose the answers: too cold, too hot, too cool and too warm was 13.51% and it is greater than 10%. That is, thermal comfort conditions could be improved in the tested rooms. However, the next figure, which shows the respondents' thermal acceptability vote, does not fully reflect the need for any improvement (Fig. 5).

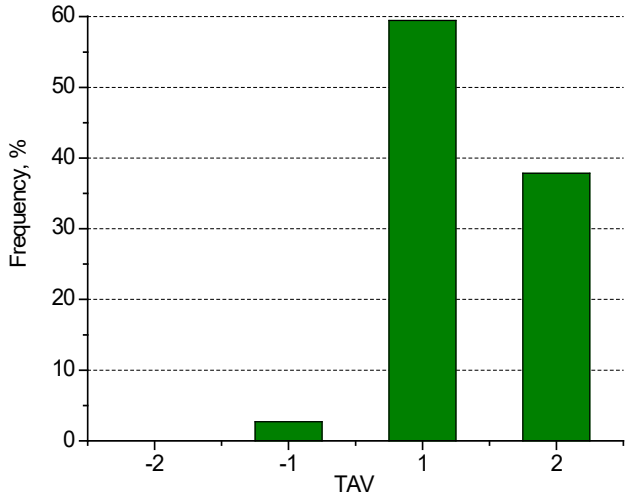

FIGURE 5. *TAV on the basis of surveys*

TAV means Thermal Acceptability Vote, which included responses in the survey: "-2" – definitely unpleasant, "2" – comfortable, "-1" – unpleasant, "1" – acceptable. TAV values were calculated as the frequency of ratings for a given response. It is worth noting that 59.46% of the surveyed assess the current temperature as acceptable. This means that 22 people (more than half of the respondents) correspond to the microclimate features in the room. Fourteen respondents assess the current temperature as comfortable, which is 37.84%. And only one person (2.70%) out of 37 respondents assessed it as unpleasant. The next parameter – namely the preferences for indoor air temperature are presented below.

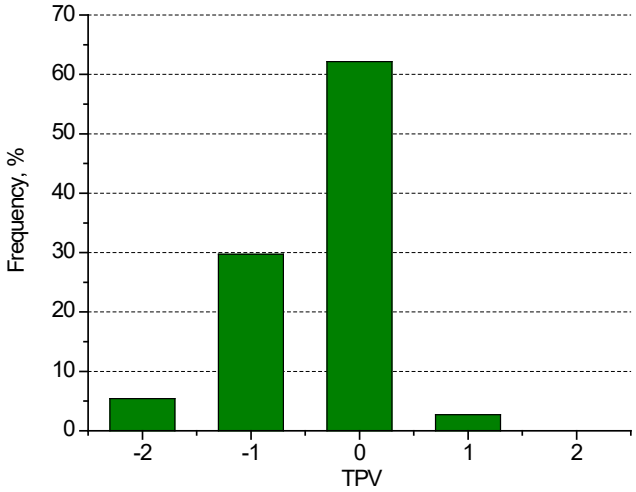

FIGURE 6. *TPV on the basis of surveys*

TPV is Thermal Preferences Vote where "-2" means definitely cooler, "2" – definitely warmer, "-1" – cooler, "1" – warmer and "0" – unchanged. TPV is the frequency of votes given for a given answer. It was observed that the respondents would like the room temperature to be unchanged. This answer was

chosen by 23 people, i.e. more than half of the respondents (62.16%). Looking at Figure 6, you can see that the preference results reflect their previous responses. Eleven volunteers want to be cooler in the room, or 29.73%. Two people want definitely cooler (5.41%) microclimate conditions, and one person (2.70%) want warmer. The article also assesses the percentage of moisture content sensations (Fig. 7).

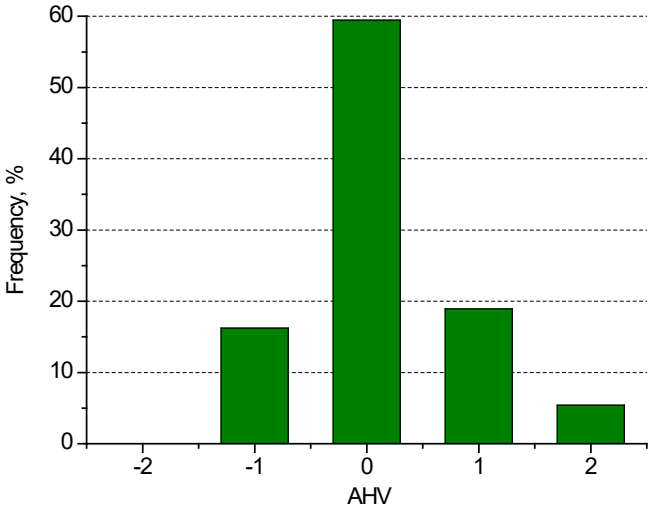

FIGURE 7. *AHV on the basis of surveys*

The graph above presents the views of respondents on the percentage rating of moisture in the indoor environment they were in. AHV means Air Humidity Vote, where "-2" is too dry, "-1" – fairly dry, "0" – pleasantly, "1" – quite damp and "2" – too humid. AHV was calculated using questionnaires as frequencies for individual responses. The vast majority chose the pleasantly answer, i.e. 59.46%. Seven people rate the humidity as quite damp, six people rate it fairly dry, and two people rate it too humid. The next chart shows their humidity preferences.

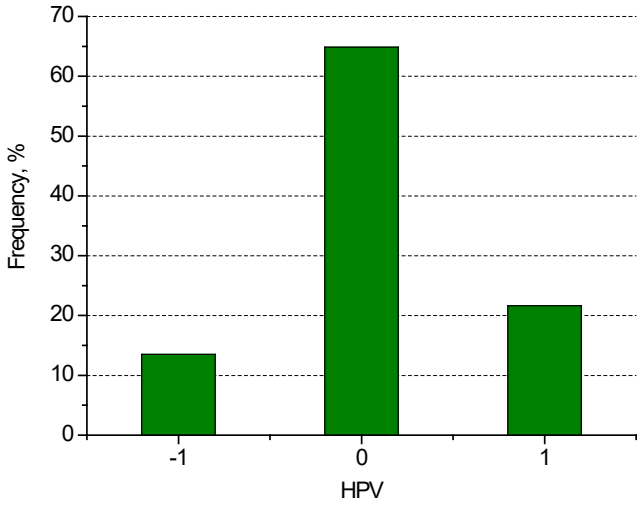

FIGURE 8. *HPV on the basis of surveys*

The y-axis indicates HPV, or Humidity Preferences Vote where "-1" means more dry, "0" – no change, "1" – more humid. In the presented graph, it can be seen that the volunteers refer to the previous graph (Fig. 7). This means that more than half of the people in the previous chart rated air humidity pleasantly. Similarly, it can be seen in the chart above that the answerers do not want modifications in air humidity (64.86% or 24 people). Eight respondents did not correspond to the humidity in the room and would like the air to be more humid (21.62%), while five people rated it as more dry (13.51%). This might be

considered surprising, because the humidity value was always in the optimal range (33-49%), so the people should not complain that the air is too humid or dry (as did about 35% of the volunteers). This means that the students were pleased with the air humidity. If the humidity was lower, the respondents would probably want the room to have a higher humidity value. Such a situation was shown in work [10]. In the opposite situation (i.e. with a high value of air humidity), the respondents would like the value of humidity to be lower. The next graph compares the thermal sensation vote of the subjects (expressed by them in the questionnaires) as TSV (the mean value of each group) with the predicted mean vote (PMV) indicator calculated according to the standard [1].

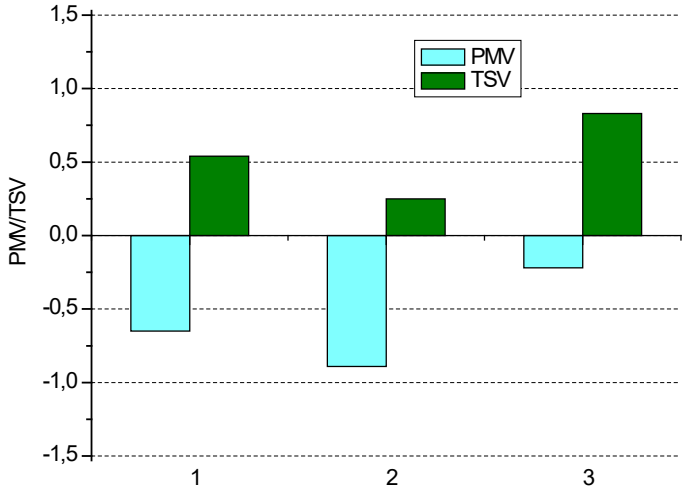

FIGURE 9. *Comparison of mean TSV comfort scores based on questionnaires and Fanger's model; 1, 2 and 3 relate to the number of the rooms*

Figure 9 compares the thermal sensation vote values with the PMV (Fanger model) values. The blue colour stands for PMV values, and green – values calculated on the basis of the surveys as the mean value for each group (each room). PMV values were calculated using the Fanger model formula. The parameters for calculating PMV (i.e., Predicted Mean Vote) were measured using the Testo 400 meter, while TSV are values calculated from anonymous questionnaires (these are the actual feelings of the people surveyed). It can be seen that these values do not match in any room. The adopted comfort range is -0.5 to +0.5. Only the second test falls within this range. The TSV for the second room is 0.25. Unfortunately, the range from the ISO 7730 standard [1] for the second room was exceeded, amounting to PMV = -0.89. The differences between TSV and PMV range from 1.05 to 1.19. The discrepancy for test spaces may depend on a number of factors that were not considered for the Fanger model such as carbon dioxide concentration or solar irradiation through windows and etc. The last graph shows the results on Predicted Percentage of Dissatisfied people with indoor conditions (calculated from surveys and taken as the mean value for each group of the people) and the Fanger model (calculation based on [1]). PPD is the percentage of the people who think that the environment is not acceptable (namely, that it falls beyond the limit of thermal acceptability and people feel too warm or too cold).

Figure 10 shows a PPD comparison computed from the questionnaires with the results computed from the Fanger model. Predicted percentage of dissatisfied (PPD) measures the expected percentage of dissatisfied people. As can be seen from the graph, it is worth noting that the predicted percentage dissatisfied (PPD) values do not coexist with the Fanger model. Only for the first room, the difference between the PPD from the surveys and the calculated value based on the Fanger model is the smallest.

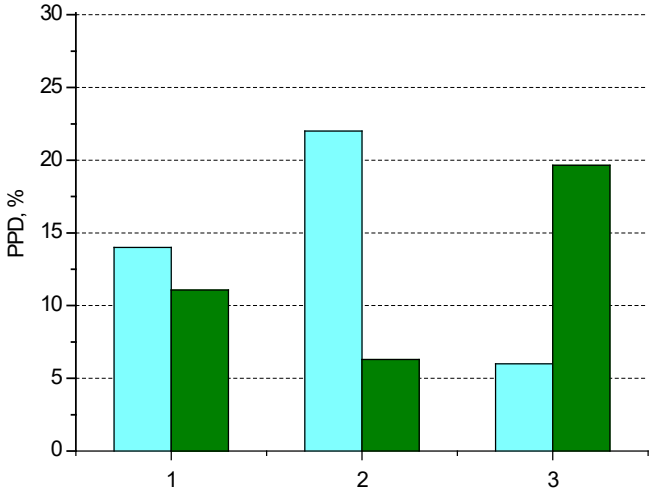

FIGURE 10. *Comparison of the PPD index calculated on the basis of the Fanger model (light blue colour) and PPD obtained on the basis of questionnaires (green colour)*

Conclusion

The presented results concerning the thermal impressions of the microclimate show that there are significant discrepancies between the mean values from the surveys and those calculated from the Fanger's model. The ISO 7730 standard [1] assumes a comfort range in the range from -0.5 to +0.5. Unfortunately, for the studied intelligent building, this range was not met, and for two out of three rooms. Besides, the PPD values were also quite high, indicated big level of dissatisfaction. To sum up, the best solution for the real values to coincide with the Fanger model is to modify the formula. Thus, it can help future designers of intelligent buildings. Providing appropriate indoor conditions is important for the health of people in the building as well as their productivity and well-being. The conducted research and analysis provided information that this building did not meet people's thermal expectations, at least in the rooms that were selected for the study and at the time of these measurements. Naturally, the results could be different for different time and different groups of people.

Acknowledgement

The work in the paper was supported by the project: "SP2023/094 Specific research in selected areas of energy processes" and "REFRESH – Research Excellence For REgion Sustainability and High-tech Industries, (VP2), (Reg. No.: CZ.10.03.01/00/22_003/0000048) co-funded by the European Union".

References

[1] ISO International Organisation for Standardization, Ergonomics of the thermal environment – Analytical determination and interpretation of thermal comfort using calculation of the PMV and PPD indices and local thermal comfort criteria, International Standard ISO 7730 (2005).

[2] PN-EN 16798-1:2019, Energy Performance of Buildings-Ventilation for Buildings-Part 1: Indoor Environmental Input Parameters for Design and Assessment of Energy Performance of Buildings Addressing Indoor Air Quality, Thermal Environment, Lighting and Acustics (2019).

[3] Fanger P.O., *Thermal comfort*, Arkady, Warsaw 1974.

[4] Becker R., Paciuk M., *Thermal comfort in residential buildings – Failure to predict by Standard model*. Building and Environment, v. 44, 2009, pp. 948-960, http://dx.doi.org/10.1016/j.buildenv.2008.06.011.

[5] Broday E.E., Moret J.A., Xavier A.A. de P., de Oliveira R., *The approximation between thermal sensation votes (TSV) and predicted mean vote (PMV): A comparative analysis*. International Journal of Industrial Ergonomics, v. 69, 2019, pp. 1-8, https://doi.org/10.1016/j.ergon.2018.09.007.

[6] Mors S.T, Hensen J.L.M. Loomans M.G.L.C., Boerstra A.C., *Adaptive thermal comfort in primary school classrooms: Creating and validating PMV-based comfort charts*. Building and Environment, v. 46, 2011, pp. 2454-2461, https://doi.org/10.1016/j.buildenv.2011.05.025.

[7] Manu S., Shukla Y., Rawal R., Thomas L.E., de Dear R., *Field studies of thermal comfort across multiple climate zones for the subcontinent: India Model for Adaptive Comfort (IMAC)*. Building and Environment, v. 98, 2016, pp. 55-70, https://doi.org/10.1016/j.buildenv.2015.12.019.

[8] Bartal I., Banhidi Hc. L., Garbai L., *Analysis of the static thermal comfort equation*. Energy and Building, v. 49, 2012, pp. 188-191, https://dx.doi.org/10.1016/j.enbuild.2012.02.005.

[9] Homoda R.Z., Sahari K.S.H., Almurib H.A.F., Nagi F.H., *RLF and TS fuzzy model identification of indoor thermal comfort based on PMV/PPD*. Building and Environment, v. 49, 2012, pp. 141-153, https://dx.doi.org/10.1016/j.buildenv.2011.09.012.

[10] Krawczyk N., Krakowiak J., *The comparison of thermal comfort test results in selected traditional and modern buildings*. E3S Web of Conferences 286, 02008, 2021, TE-RE-RD, https://doi.org/10.1051/e3sconf/202128602008.

[11] Majewski G., Telejko M., Orman Ł.J., *Preliminary results of thermal comfort analysis in selected buildings (EKO-DOK)*, Poland, E3S Web of Conferences, 17, 00056, 2017, https://doi.org/10.1051/e3sconf/20171700056.

[12] Piotrowski J.Zb., Orman Ł.J., Lucas X., Zender-Świercz E., Telejko M., Koruba D., *Tests of thermal resistance of simulated walls with the reflective insulation*. Czech Republic, EPJ Web of Conferences, v. 67, 2014, 02095, https://doi.org/10.1051/epjconf/20146702095.

[13] Vilcekova S., Meciarova L., Burdova E.K., Katunska J., Kosicanova D., Doroudiani S., *Indoor environmental quality of classrooms and occupants' comfort in a special education school in Slovak Republic*. Building and Environment, v. 120, 2017, pp. 29-40, http://dx.doi.org/10.1016/j.buildenv.2017.05.001.

[14] Zhang W., Liu F., Fan F., *Improved thermal comfort modeling for smart buildings: A data analytics study*. International Journal of Electrical Power and Energy Systems, v. 103, 2018, pp. 634-643, https://doi.org/10.1016/j.ijepes.2018.06.026.

[15] Jindal A., *Thermal comfort study in naturally ventilated school classrooms in composite climate of India*. Building ana Environment, v. 142, 2018, pp. 34-46, https://doi.org/10.1016/j.buildenv.2018.05.051.

[16] Yuan F., Yao R., Sadrizadeh S., et. al., *Thermal comfort in hospital buildings – A literature review*. Journal of Building Engineering, v. 45, 2022, 103463, https://doi.org/10.1016/j.jobe.2021.103463.

[17] Rahman N.M.A., Haw L.Ch., Fazlizan A., Hussin A., Imran M.S., *Thermal comfort assessment of naturally ventilated public hospital wards in the tropics*. Building and Environment, v. 207, 2021, 108490, https://doi.org/10.1016/j.buildenv.2021.108480.

[18] Dębska L., Krakowiak J., *Thermal comfort analysis in the sustainable educational building*. Second International Conference on Sustainable Futures: Environmental, Technological, Social and Economic Matters (ICSF 2021), 280, 2021, https://doi.org/10.1051/e3sconf/202128004011.

Andrii CHEILYTKO

German Aerospace Center (DLR), Institute of Solar Research, Julich, Germany

Corresponding author: andrii.cheilytko@dlr.de

Doi: 10.53412/jntes-2023-2-2

A NEW IDEA TO INCREASE THE CONVECTIVE EFFICIENCY OF A SOLAR TOWER AIR RECEIVER BY CREATING A CONTROLLED VORTEX

Abstract: *Concentrated solar energy as a source of renewable energy has a high potential for solving the current energy crisis. The solar tower receiver is a crucial element of solar energy conversion efficiency. To increase the convective efficiency of the solar tower receiver, the idea of creating a vortex is proposed. The vortex is created either in the plane in front of the receiver, for flat receivers, or in the internal volume of the receiver, for cavity-type receivers. The calculation formulas for calculating the parameters of the controlled vortex are proposed and computer modeling is performed to determine the effectiveness of the proposed idea. The results of computer modeling confirmed the physical possibility of the controlled vortex formation in the receiver space and visually show the flow structure. Also, the general dependence of the air return coefficient in the VoCoRec receiver on the flow twist was found. Conclusions are drawn on the satisfactory results obtained and on the improvement of the existing model of the controlled vortex.*

Keywords: *receiver, solar tower, convective efficiency, vortex, modeling, air return ratio*

Introduction

Solar energy is widely used for the production of low potential heat and for the production of electricity. In the first case, flat solar collectors are used that do not concentrate (coolant – water, air, antifreeze). In the second – electricity from the light flux can be produced in two ways: by direct conversion in photovoltaic installations or by heating the coolant, which performs work in a thermodynamic cycle. Concentrated solar power plants (CSP) are used to use high potential thermal energy.

Energy and exergy efficiency of different CSP elements (turbine, generator, pumping group) is above 90%. The energy efficiency of the receiver does not reach 90%, and the exergy efficiency is at best 60%. Therefore, it is possible to achieve the highest efficiency with the lowest economic investment by improving the CSP receiver technology.

The efficiency of the receiver in a stationary process depends only on the ratio of changes in the thermal energy of the fluid to the supplied solar energy. This formulation of the problem allows to calculate the overall efficiency of the receiver, but does not allow to optimize its structure. Therefore, for the problem of improving the structure of the receiver, it is necessary to adhere to the following initial factors of the model: efficiencies based on receiver spillage; efficiencies based on receiver absorption; efficiencies based on receiver radiation; efficiencies based on receiver convection; efficiencies based on receiver conduction.

In this article, we propose to consider the idea of increasing the efficiency based on receiver convection in open-type receivers of solar towers by creating a controlled vortex.

Literature revive

As a rule, the efficiency of the receiver is found by the numerical model without dividing it into components [1, 2]. But this approach does not make it possible to analyze the dependent factors of influence on the receiver of the solar station, so for the modeling of the receiver it is considered as its indicators. The efficiency of an open receiver as the efficiency of its elements [3]. According to this approach, the convective losses of the receiver will be determined separately from other components of the thermal efficiency of the solar tower receiver.

The problem of warm air leakage from the tmp cavity receiver has been known since the end of the last century [4]. But for the first time a broad overview of 18 proposals to reduce warm air leakage with an assessment of these measures appeared in 2014 in the work of J. Grobbel [5]. The idea of barrier flow is to prevent hot air from leaving the opening and cold air from entering it, and can be compared to an air curtain on a building door. One idea is to blow to cancel the existing vortex in the receiver. Another is to introduce an additional vortex, and so on. At the same time, the author did not consider the idea of creating a controlled vortex with specific sealing characteristics that will depend on the mass.

Among the modern works that investigate the problems of increasing the air return coefficient, it is worth noting the works of [6-9] which consider both analytical and practical methods for calculating heat losses with exhaust air, as well as the dependence of the air return coefficient on the angle of the receiver to the horizon. However, none of these studies considered the possibility of increasing the convective efficiency of the receiver by creating a controlled vortex. Therefore, the idea of creating a controlled vortex is considered new and is discussed in more detail in this article.

Theory and calculation

To understand the cause of air leakage, it is necessary to consider its aerodynamics. The relationship between the velocity and pressure field is described by the Navier-Stokes equations [10]

$$\nabla\left(-p+\mu\left(\nabla w+\left(\nabla c w^{T}\right)\right)\right)=\rho\left(w\nabla\right)w \tag{1}$$

where:
w – speed.

The optimal configuration of the receiver cannot be calculated separately and is considered in conjunction with other parts of the solar tower [11]. Therefore, consider the balance of the receiver as a block with input and output parameters. Considering the energy balance of the air circuit of a solar tower with an open porous receiver, it is possible to write down the direct circuit efficiency

$$\eta_{rec}^{air}=\frac{Q_{use}^{air}}{I_{rec}} \tag{2}$$

where:

Q_{use}^{air} – the heat energy transferred from the primary air heat transfer medium to the next circuit is defined as the difference in enthalpy between the air at the inlet and outlet of the heat exchanger or reactor in which the energy is transferred, kW;

and inverse balance

$$\eta_{csp}^{air}=\frac{I_{mirror}-Q_{loss}^{air}-Q_{refl}^{rec}-Q_{emi}^{rec}-Q_{h.tr}^{CSP}-Q_{loss}^{mirror}-W_{fan}}{I_{mirror}} \tag{3}$$

$$I_{mirror}-Q_{loss}^{air}-Q_{refl}^{rec}-Q_{emi}^{rec}-Q_{h.tr}^{CSP}-Q_{loss}^{mirror}=\Delta H_{f} \tag{4}$$

where:

Q_{loss}^{air} – energy loss with the physical heat from the air leaving the solar plant to the environment, kW;

Q_{refl}^{rec} – energy loss by reflection of solar radiation in the porous absorber into the environment, kW;

Q_{emi}^{rec} – energy loss by emission (convective and radiation losses) in the porous absorber to the environment, kW;

$Q_{h.tr}^{CSP}$ – heat loss from the air circuit surface of the solar tower pipe and heat exchange to the environment, kW;

Q_{loss}^{mirror} – losses of solar energy from uneven arrival of solar radiation from mirrors, kW;

W_{fan} – power for internal air circuit needs, in the simplest case this is fan operation, kW;

or in relative terms

$$\eta_{csp}^{air} = 1 - q_{loss}^{air} - q_{refl}^{rec} - q_{emi}^{rec} - q_{h.tr}^{CSP} - q_{loss}^{mirror} - K_w \tag{5}$$

this

$$q_{loss}^{air} = \frac{Q_{loss}^{air}}{I_{mirror}};\quad q_{emi}^{rec} = \frac{Q_{emi}^{rec}}{I_{mirror}};\quad q_{h.tr}^{CSP} = \frac{Q_{h.tr}^{CSP}}{I_{mirror}};\quad q_{loss}^{mirror} = \frac{Q_{loss}^{mirror}}{I_{mirror}};\quad K_w = \frac{W_{fan}}{I_{mirror}} \tag{6}$$

Energy loss with the physical heat from the air leaving the solar plant to the environment, kW

$$Q_{loss}^{air} = \left(H_{loss}^{air} - H_{amb}^{air}\right)\cdot\left(1 - ARR\right)\cdot\varepsilon \tag{7}$$

where:

H_{loss}^{air} – enthalpy carried with air, kJ/s;

H_{amb}^{air} – enthalpy brought in with ambient air, kJ/s;

ARR – air return ratio;

ε – a delay factor related to the time required to heat the exhaust air to a given temperature, for the stationary case = 1.

Considering that the ratio of receiver air losses is directly proportional to the change in *ARR*, ceteris paribus, energy losses with air

$$\frac{Q_{loss}^{air}|_{ARR1}}{Q_{loss}^{air}|_{ARR2}} = \frac{1 - ARR|_1}{1 - ARR|_2} \tag{8}$$

$$Q_{loss}^{air}|_{ARR2} = Q_{loss}^{air}|_{ARR1}\,\frac{1 - ARR|_2}{1 - ARR|_1} \tag{9}$$

The efficiency ratio can be written as

$$\frac{\eta_{conv}|_{ARR1}}{\eta_{conv}|_{ARR2}} = \frac{\Delta U_{rec} + \Delta H_f + Q_{loss\_en} + Q_{loss}^{air}|_{ARR2}}{\Delta U_{rec} + \Delta H_f + Q_{loss\_en} + Q_{loss}^{air}|_{ARR1}} \tag{10}$$

Therefor

$$\frac{\eta_{conv}|_{ARR1}}{\eta_{conv}|_{ARR2}} = \frac{1+\frac{\eta_{cond}Q_{loss}^{air}|_{ARR2}}{I_{mirror}\eta_{rec}^{air}}}{1+\frac{\eta_{cond}Q_{loss}^{air}|_{ARR1}}{I_{mirror}\eta_{rec}^{air}}} \tag{11}$$

$$\frac{\eta_{conv}|_{ARR1}}{\eta_{conv}|_{ARR2}} = \frac{1+\frac{\eta_{cond}Q_{loss}^{air}|_{ARR1}\frac{1-ARR|_2}{1-ARR|_1}}{I_{mirror}\eta_{rec}^{air}}}{1+\frac{\eta_{cond}Q_{loss}^{air}|_{ARR1}}{I_{mirror}\eta_{rec}^{air}}} \tag{12}$$

$$\frac{\eta_{conv}|_{ARR2}}{\eta_{conv}|_{ARR1}} = \frac{1+q_{loss}^{air}|_{ARR1}\cdot\frac{\eta_{cond}}{\eta_{rec}^{air}}}{1+q_{loss}^{air}|_{ARR1}\cdot\frac{\eta_{cond}}{\eta_{rec}^{air}}\cdot\frac{1-ARR|_2}{1-ARR|_1}} \tag{13}$$

$$q_{loss}^{air}|_{ARR1}\left\langle 1,\frac{\eta_{cond}}{\eta_{rec}^{air}}\right\rangle 1 \tag{14}$$

To determine the change in the convective efficiency of the swirling efficiency flow, a computer simulation of the VoCoRec receiver was performed. The twisting process for each face of the receiver is shown in Figure 1.

Each kg of dry air contains 125.98 kJ/kg of energy at 5 bar and 150°C and 832.48 kJ/kg at 800°C [12]. Achieving an *ARR* from 0.6 to 0.9 allows the system to feedback approx. 38 kJ/kg of energy. The practical target for improvement of the new model is to achieve an *ARR* above 0.9, therefor $q_{loss}^{air}|_{ARR=0.9} = 0.05$. A modern model of an absorber like VoCoRec allows for an *ARR* of 0.9. For a typical calculation of the energy efficiency of a solar tower with volumetric receiver of open type, it is customary to take $I_{mirror} = 1000\ \mathrm{kW/m^2}$ flux density in the aperture plane and 800°C hot air temperature [13], $\Delta H_f = 1000$ kJ/kg [14-16].

If

$$\frac{\eta_{cond}}{\eta_{rec}^{air}} = 1.125$$

then

$$\frac{\eta_{conv}|_{ARR2}}{\eta_{conv}|_{ARR=0.9}} = \frac{1.05625}{1+0.05625\cdot\frac{1-ARR|_2}{0.1}} \tag{15}$$

Therefore, an increase of *ARR* from 0.9 to 0.95 will increase efficiency by 1.027 times.

There are a number of studies dedicated to the study of cyclone devices: studies of methods for determining the resistance coefficient, studies of methods for determining the angle of twist, studies of methods for determining the zone of reverse currents [17, 18].

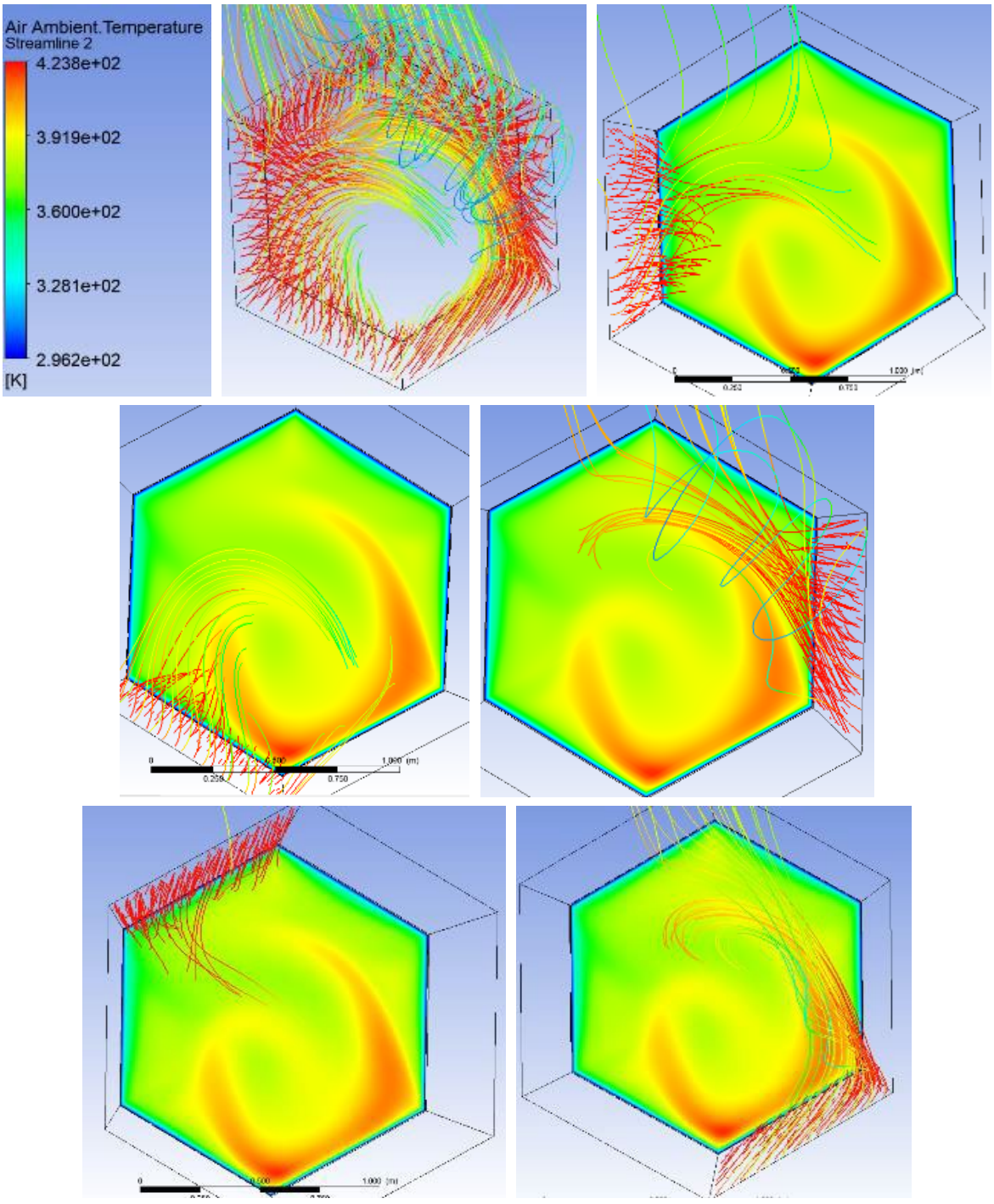

FIGURE 1. *Temperature distribution along current lines for swirling flow in VoCoRec Large mass Flow 2.43 kg·s^{-1}*

Finding the zone of inverse currents is given in [17] where the vortex radius is proposed to be found from the "radius of twist of the flux" which is defined as

$$\alpha = \arcsin \sqrt[3]{\frac{\sum f_{BX}}{\pi \cdot R_n \cdot R_c \cdot \cos\beta \cdot \cos\gamma} \cdot \frac{1}{4\xi}} \tag{16}$$

where:

ξ – the ratio of the initial momentum loss;

β, γ – for a shovel-less certifier are assumed to be equal to zero;

R_c – aerodynamic camera resistance;

R_n – aerodynamic nozzle resistance.

Air output momentum

$$M_{out}=\int_0^{2\pi}\int_{R_V}^{R_{Out}}\rho_{out}W_{out}^2\sin\alpha_1\cos\alpha_1 r^2 dr d\varphi \tag{17}$$

The size of the inverse current zone is proposed to be defined as

$$\frac{R_B}{R_C}=1-\frac{\sum f_{BX}}{\pi\cdot R_K\cdot R_C\cdot\cos\beta\cdot\cos\gamma}\cdot\frac{1}{2\mathrm{tg}\alpha}\cdot\frac{1}{\xi}\cdot\frac{\rho_0}{\rho_1} \tag{18}$$

The resistance of the swirl unit is characterized by the resistance coefficient

$$\xi=\frac{2\Delta P}{\rho w^2} \tag{19}$$

where:

w – the average flow rate;
ρ – the flux density at the same location;
ΔP – the difference between the pressure at the inlet and outlet of the swirl unit.

$$\xi\left(ARR=1\right)\rightarrow\min \tag{20}$$

Decomposing the velocity vector into components we obtain

$$w^2=c^2+u^2+v^2 \tag{21}$$

where:

c – tangential speed;
u – radial speed;
v – axial speed.

Figures 2 and 3 show the temperature distribution of the swirling flow for different mass flow rates. From the figures, it can be seen that the mass flow rate affects not only the formation of the vortex in the aorta but also its uniformity of distribution.

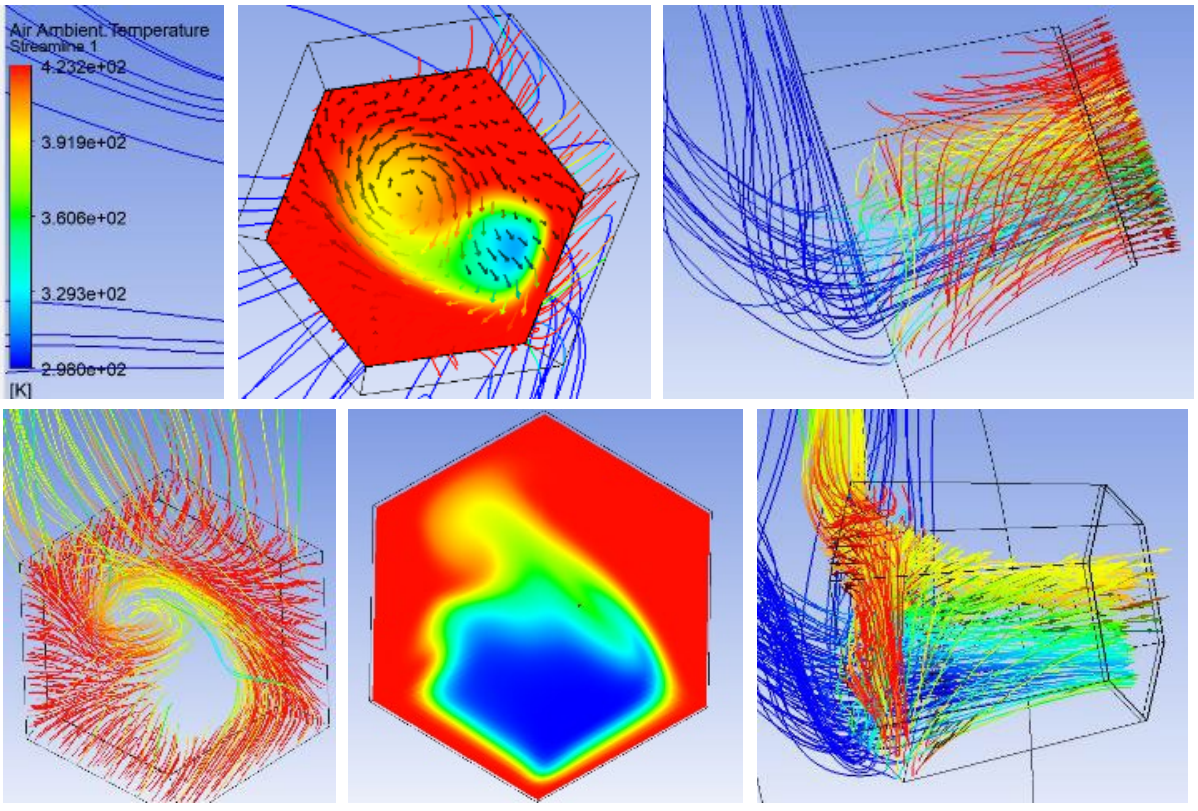

FIGURE 2. *Temperature distribution along current lines for swirling flow in VoCoRec Large mass Flow 5.04017 kg·s^{-1}*

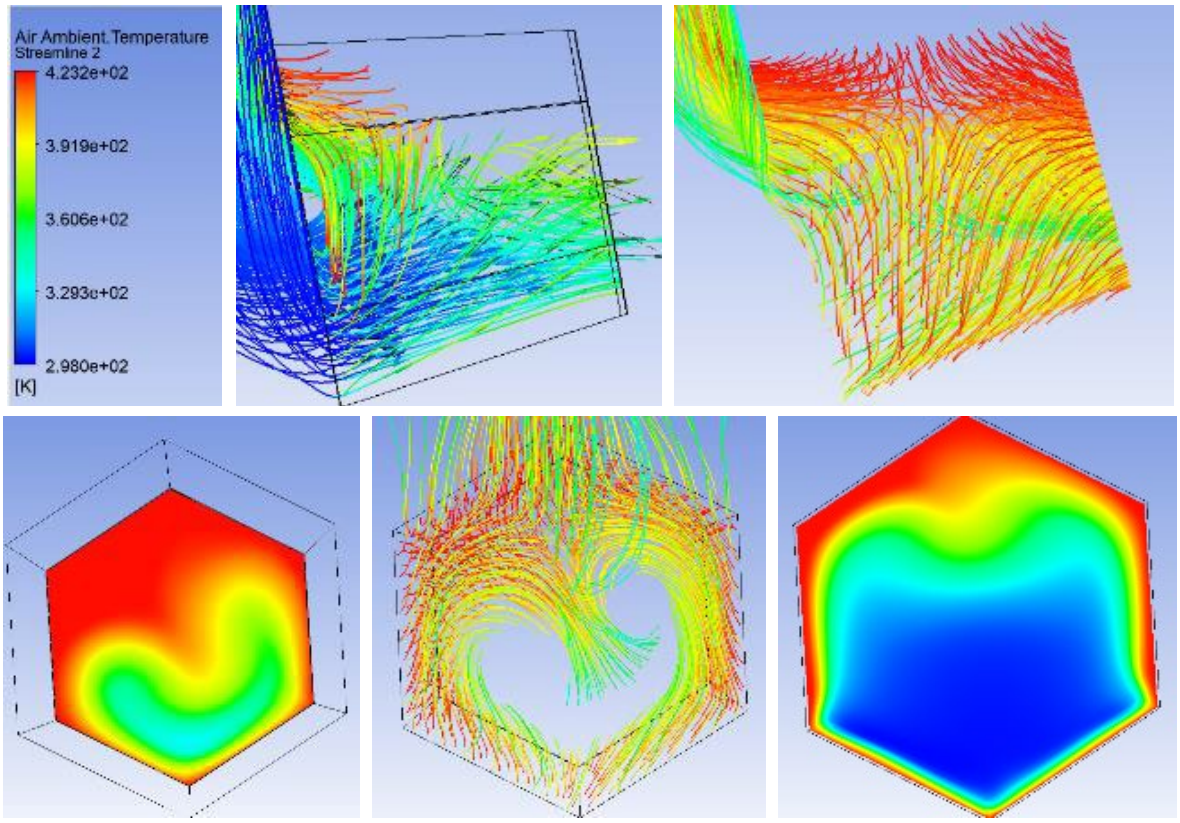

FIGURE 3. *Temperature distribution along current lines for swirling flow in VoCoRec Large mass Flow 1.2 kg·s^{-1} ARR = 0.7*

Boundary conditions for air by front absorber in the absence of traction forces to the main absorber, vector v of directions towards the main absorber

$$r \in \left(0; R_{abs}\right) \tag{22}$$

If

$$r \in \left(0; r_{in}\right)$$

then

$$\text{grad}(\text{P}) < 0,\ c > 0,\ v \to 0,\ v < 0$$

in the separated line:

if

$$r = R_V$$

then

$$v = 0;\ \text{grad}(\text{P}) = 0,\ c = 0$$

if

$$r = \left(R_V; R_{abs}\right)$$

then

$$\text{grad}(\text{P}) > 0,\ v > 0,\ c > 0,\ u > 0$$

It is proposed to find the function of aerodynamic resistance as well as the air return coefficient using computer modeling. The air return coefficient is calculated as the ratio of the air that exited the receiver and entered the main absorber to the total mass flow rate through the main absorber.

Comparing the air velocity fields in the receiver for different mass flow rates with and without flow swirl (Fig. 4), it was concluded that the line of zero velocity gradient (flow separation line) with flow swirl shifts to the receiver aperture.

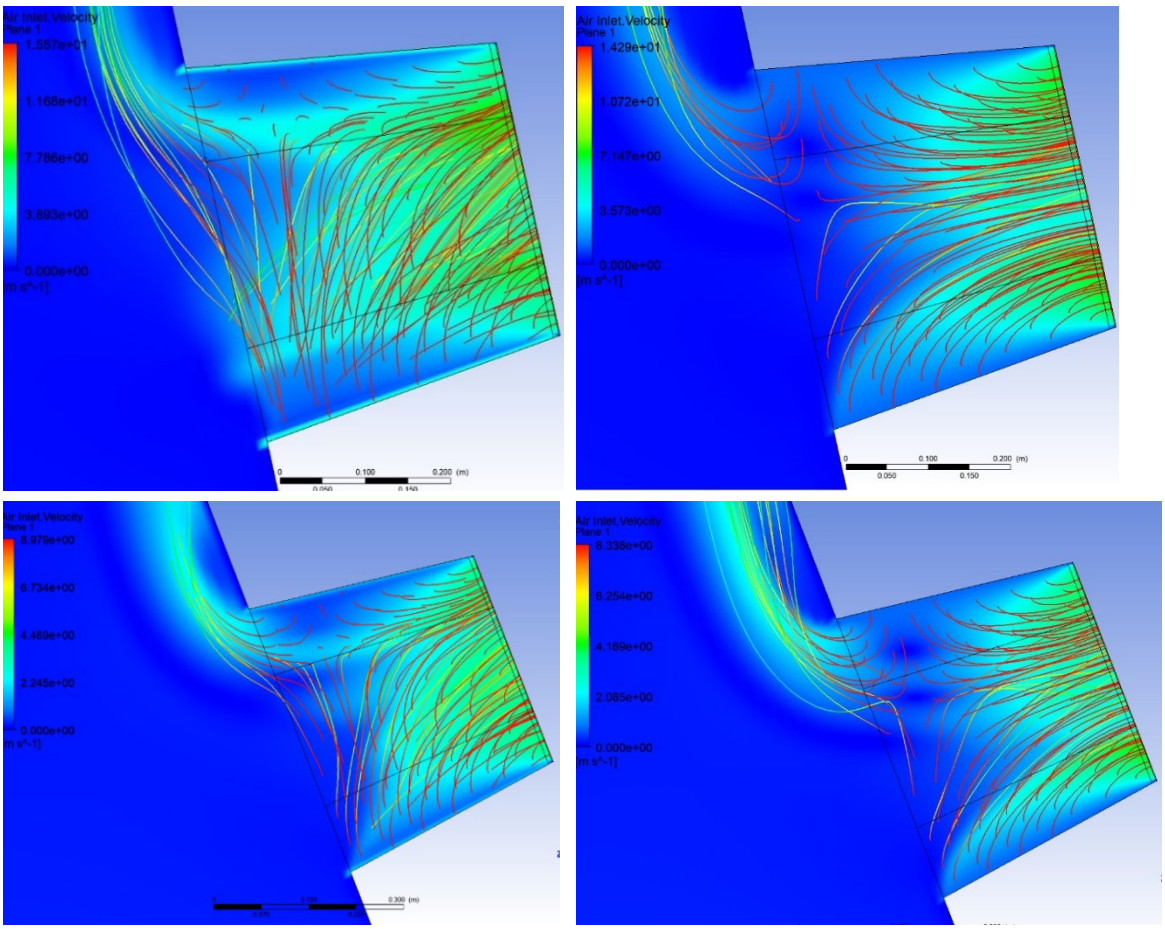

FIGURE 4. *Air inlet velocity in VoCoRec small size with m = 0.21 kg·s^{-1}, VGR = 0.6, ARR = 0.871 (left up) and m = 0.21 kg·s^{-1}, VGR = 1, ARR = 0.935 (right up) and m = 0.12 kg·s^{-1}, VGR = 0.7, ARR = 0.872 (left down) and m = 0.12 kg·s^{-1}, VGR = 1, ARR = 0.87 (right down)*

The Figure 5 shows the distribution of air temperature near the front of the main absorber, which provides conditions for analyzing the occurrence of local overheating points.

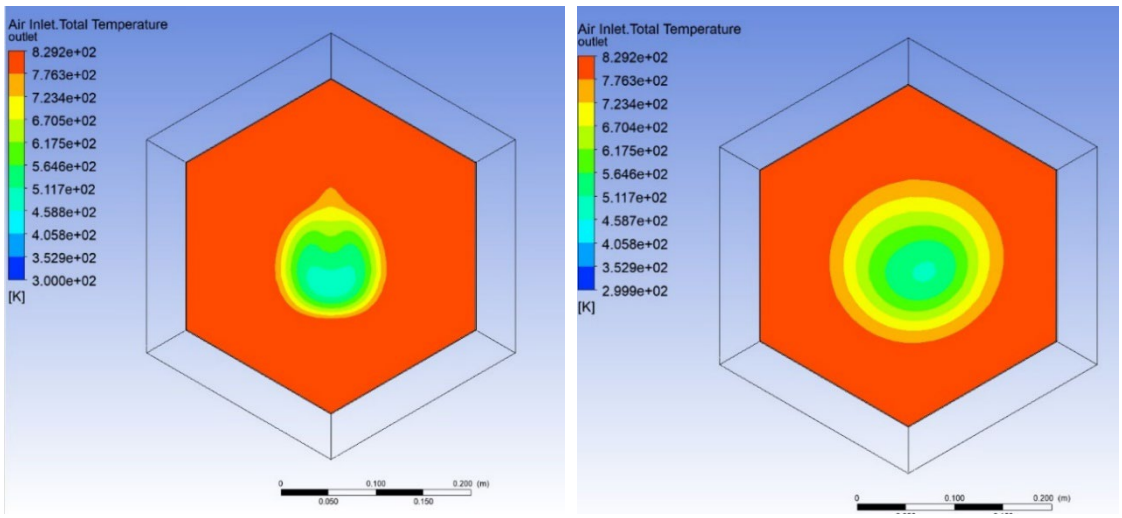

FIGURE 5. *Air outlet temperature in VoCoRec small size with m = 0.21 kg·s^{-1}, VGR = 0.6, ARR = 0.871 (left) and m = 0.21 kg·s^{-1}, VGR = 1, ARR = 0.935 (right)*

Figure 5 shows that for a given mass flow rate, the air return coefficient decreased with the flow swirl, and the thermal drop across the main absorber increased. Although the flow was distributed more evenly, it created a cold spot in the center of the absorber due to the strong reverse flow zone.

Structurally, the swirling flow can be achieved by: tangential air supply or by installing guide vanes.

The change in *ARR* from a decrease in the radial component with an increase in the tangential component (i.e., stronger flow twist) for low mass flow is shown in Figure 6.

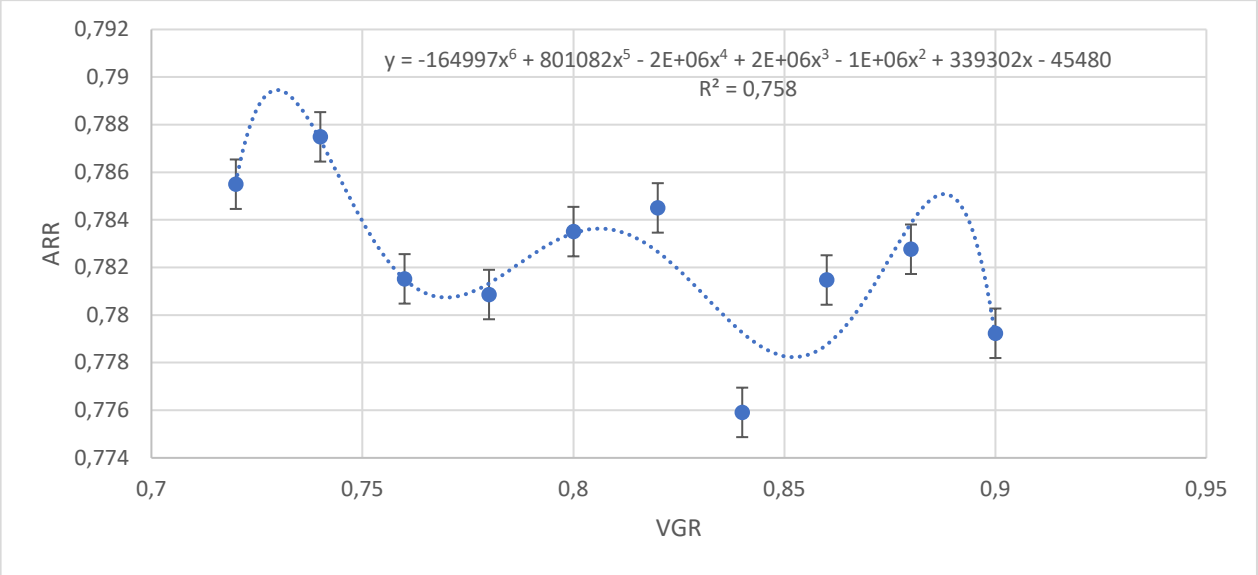

FIGURE 6. *Dependence of ARR on the radial component of the vector gradient (VGR) in the flow direction 2.43 kg·s^{-1} of the VoCoRec Large*

These results indicate a general tendency to increase the air return ratio, and hence the convective efficiency of the receiver when creating a controlled vortex. However, the results also show significant fluctuations in the *ARR* from the radial component of the air supply to the receiver zone caused by the high degree of turbulence.

Conclusions

This paper considers the possibility of creating a controlled vortex in an open-type receiver of a solar tower. The basic solution dependencies are proposed and the vortex structure in the modeled flow is shown. In order to increase the convective efficiency of the receiver, it is necessary to reduce the aerodynamic drag of the receiver structure and to reduce the air return coefficient.

A high degree of dependence of the air return coefficient on the mass flow rate through the receiver has been confirmed. The polynomial dependence of the air return coefficient in the receiver on the radial component of the circulating air velocity is shown. It is proved that the existence of a vortex can have both positive and negative results. In order to develop an analytical model, it is proposed to conduct comprehensive studies of the dependencies of the air return coefficient on the components of velocity and mass flow rate.

Most importantly, the possibility of increasing the convective efficiency of the solar thermal receiver by 2% by creating a controlled vortex was confirmed.

References

[1] Ni X.W., Liu T.N., Liu D., *Effects of Volumetric Property Models on the Efficiency of a Porous Volumetric Solar Receiver*. Energies, 2022, 15(11). DOI: 10.3390/en15113899.

[2] Jayranaiwachira N., et al., *Thermal-hydraulic performance of solar receiver duct with inclined punched-ribs and grooves*. Case Studies in Thermal Engineering, 2022, 39. DOI: ARTN 10243710.1016/j.csite.2022.102437.

[3] Hoffschmidt B., et al., *High Concentration Solar Collectors*. Reference Module in Earth Systems and Environmental Sciences, 2021.

[4] Becker M., et al., *Second generation central receiver technologies*. 1993, Karlsruhe (Germany): C.F. Mueller; Deutsche Forschungsanstalt fuer Luft- und Raumfahrt e.V. (DLR), Koeln (Germany); Sandia National Labs., Albuquerque, NM (United States). 133.

[5] Grobbel J., *Development and Numerical Investigation of Reduction Strategies for Convective Heat Losses of Cavity Receivers Used in Solar Thermal Power Towers*, in Faculty of Mechanical Engineering Chair of Solar Technology. 2014, FH Aachen. p. 89.

[6] Drexelius M., Schwarzbözl P., Pitz-Paal R., *Experimental evaluation of wind induced pressure fluctuations in cavity shaped open volumetric air receivers*. Solar Energy, 2022, 247: p. 146-157. DOI: https://doi.org/10.1016/j.solener.2022.10.003.

[7] Busch K., et al., *VoCoRec – Design and performance of the two-stage volumetric conical receiver*, in SolarPACES 2022, 2022, Solar Power and Chemical Energy Systems: U.S.A., Albuquerque.

[8] Stadler H., et al., *CFD model for the performance estimation of open volumetric receivers and comparison with experimental data*. Solar Energy, 2019, 177: p. 634-641. DOI: 10.1016/j.solener.2018.11.068.

[9] Maldonado D., et al., *Evaluation of Aim Point Optimization Methods*. International Conference on Concentrating Solar Power and Chemical Energy Systems (Solarpaces 2017), 2018, 2033. DOI: Artn 040025-1 10.1063/1.5067061.

[10] Capuano R., et al., *Innovative Solar Receiver Micro-Design Based on Numerical Predictions*, in ASME 2015 IMECE. 2015: Houston, USA.

[11] Davis D., et al., *Thermal performance of vortex-based solar particle receivers for sensible heating*. Solar Energy, 2019, 177: p. 163-177. DOI: 10.1016/j.solener.2018.10.086.

[12] VDI Heat Atlas. 2 ed. VDI-Buch. 2010: Springer Berlin, Heidelberg. XLII, 1584.

[13] Offergeld M., et al., *VoCoRec – a Novel Two-Stage Volumetric Conical Receiver*, in SolarPACES, 2021.

[14] PitzPaal R., et al., *Experimental and numerical evaluation of the performance and flow stability of different types of open volumetric absorbers under non-homogeneous irradiation*. Solar Energy, 1997, 60(3-4): p. 135-150. DOI: Doi 10.1016/S0038-092x(97)00007-8.

[15] Gomez-Garcia F., et al., *Thermal and hydrodynamic behavior of ceramic volumetric absorbers for central receiver solar power plants: A review*. Renewable and Sustainable Energy Reviews, 2016, 57: p. 648-658. DOI: https://doi.org/10.1016/j.rser.2015.12.106.

[16] Rosenstiel A., et al., *Electrochemical Hydrogen Production Powered by PV/CSP Hybrid Power Plants: A Modelling Approach for Cost Optimal System Design*. Energies, 2021, 14(12). DOI: ARTN 3437 10.3390/en14123437.

[17] Golubtsov V.M., *To the calculation of the resistance coefficient of single-chamber cyclone furnaces*. Heat power engineering, 1978, 4: p. 78-80.

[18] Cheilytko A., Pavlenko A.M., Koshlak H., *Features of dispersed flow hydrodynamics in vortex chambers*. A collection of research papers from the DSTU, 2010, 11: p. 76-82.

Karolina SADKO
Kielce University of Technology, Poland
Corresponding author: ksadko@tu.kielce.pl

Doi: 10.53412/jntes-2023-2-3

EXPERIMENTAL ANALYSIS OF HEAT FLUX DISTRIBUTION IN TRIPLE-PANE WINDOWS WITHIN A CLIMATIC CHAMBER

Abstract: *An experimental study was carried out to investigate the heat flux distributionon the external surface of triple-pane windows under various conditions including: outdoor temperatures, gas filling, emissivity of the glass surfaces, and the use of electrical heating. The measurements were conducted within a controlled climatic chamber. Two window configurations were examined: one filled with air (emissivity of ε = 0.84) and the other filled with argon (emissivity of ε = 0.17). In addition, the study also assessed the impact of a local and surface electric heating on heat loss. The key contribution of this researchlies in revealing variations in the heat flux density across different parts of the external glazing of each window, specifically the lower, central, and upper regions. These findings emphasize the importance of considering the non-uniformity of thermal resistance in different areas of windows in order to accurately determine their heat transfer coefficient.*

Keywords: *heat transfer, heat flux, windows, triple-pane windows, thermal transmittance*

Introduction

Windows and glazed facades are crucial components of building sthat impact the energy efficiency, visual and acoustic comfort of residents as well as thermal performance. However, up to 60% of total heat loss through the building envelope can be attributed to the glazed areas due to their comparably higher overall heat transfer coefficient (*U*-value) [1]. Therefore, enhancing the thermal resistance (*R*-value) of glazed building partitions holds great potential for substantial increase of energy savings.

One of the possible ways of decreasing the thermal transmittance of windows is the utilization of triple-pane windows. The thermal resistance of a triple-pane window filled with air is approximately 1.7 times higher than that of a double-pane window of the same size [2]. The central pane in the triple-pane window causes reduction in velocity of free-convective flow of gas in the gap between panes resulting in higher thermal resistance. As gas rises along the room-side pane surface facing the gap, it changes the flow direction in the upper part of the window and descends along the cold pane surface facing the gap, thus creating a primary circulation. Moreover, micro-convection in the form of secondary multicellular circulations occurs in the gaps of multi-pane windows at the critical Rayleigh number values, therefore causing the degradation of linear temperature profiles. It was found that the Rayleigh number, at which a multicellular flow occurs, is ranging from 6.070 to 6.740 [3]. A similar conclusion was established in paper [4]. The suppression of multicellular flow in the layers of gas between panes occurred when the number of panes increased from two to three. The lower temperature gradient between cavity surfaces was observed in triple-pane windows, resulting in the reduction of buoyancy force in the gas layers. Additionally, the central pane behaves as a screen, decreasing the radiative heat exchange. Another solution to reduce the heat transfer by radiation is an application of low emissivity coatings to the pane surfaces [5]. Replacing air with low thermal conductivity gases such as argon to fill the window gaps can lead to the reduction of conductive and convective heat fluxes [6]. The distribution of the density of heat

fluxes on the glazing surfaces is therefore influenced by the phenomena of convection, conduction and radiation, as well as the materials used in the windows. The level of heat flow passing through the area closest to the window edges differs significantly from the one most proximal to the central area. Both the materials used for making window frames as well as those utilized in the production of insulating layers between the panes in the areas near the glass edges have a higher thermal conductivity than the gas layers in the gaps between the panes. As a consequence, the *U*-value is not exclusively dependent on the window's surface area, but on the ratio between the central glazed area and the peripheral section [7]. The energy saving that could be achieved by replacing double-pane windows with triple, and quadruple-pane windows was studied in paper [8]. It has been proven that the temperature difference and the number of panes had a greater impact on the heat flux densities than the width of the gap between the panes. A glazing distance of 18 mm in combination with an external temperature of 5°C resulted in an almost 150 W/m^2 heat loss measure for a double-pane window, dropping to 70 W/m^2 for a triple-pane window. The decrease was even more not able when an external temperature amounted to 15°C. In that instance, the heat loss was reduced from 200 W/m^2 to 90 W/m^2 for a triple-pane window. However, the heat fluxes were obtained for the average and constant values of the inner and outer pane surface temperatures. It was possible due to the fact that convective heat transfer resistance in the inner and outer panes was not considered. Aguilar-Santana et al. utilized the heat flux meter method (ISO 9869-1:2014) to investigate temperatures and heat flow on the glazing surface of active insulated windows [9]. Experimental tests were carried out using the heat flux meters attached to the center of the pane. Furthermore, three temperature stations were placedat the window edges in order to assess the thermal transmittance in the weakest points of tested windows. The results showed that, for an interior chamber temperature of approximately 3.0°C and an external ambient temperature of 12.0°C, the heat flux through the central part of argon-filled double-pane window ranged from 22 W/m^2 to 28 W/m^2, resulting in a *U*-value of 3.09 W/m^2·K. Moreover, the measurements confirmed higher thermal transmittance near the lower and upper areas of each window. The highest *U*-value of 1.48 W/m^2·K was registered at the top corner station of the tested vacuum window, whilst the bottom corner stationrecorded 1.33 W/m^2·K. Thus, compared to the central part of the window, where the measured *U*-value was 1.12 W/m^2·K, the values obtained in the upper and lower parts were 32% and 19% higher, respectively. Similarly, Cuce's research [10] on argon-filled double-pane windows in environmental chamber tests revealed varying *U*-values of 1.25, 1.18 and 1.32 W/m^2·K for the top, center, and lower parts of the window, respectively, emphasizing the influence of boundary effects and thermal bridges on heat flux density distribution. The lowest values of the heat flux density in the central part of the window were also confirmed by experimental studies carried out by Pavlenko and Sadko [11]. The study analyzed heat flow patterns in windows with electric heating in an occupied house, considering the operating temperature, location, and orientation [12]. It also compared temperature and dew point distribution profiles with input power values set accordingly to the varying operating temperature conditions of the heated glazing. The influence of solar irradiation resulted in diverse heat flow patterns, and temperature sensor measurements exhibited significant differences from the average temperature at the center of the heated window. The heat flux distribution for each pane of triple-glazed supply-air window was experimentally estimated in [13]. It was pointed out that due to the high thermal conductivity of glass, relying solely on thermocouples is inadequate. However, using heat flux meters at different window heights made it possible to determine the variation of heat flux in different parts of the glazing surface. In situ measurements are widely employed to evaluate the actual thermophysical properties of building elements, offering higher accuracy than other approaches, mainly based on tabulated data. However, this method's extensive financial and time requirement limit its widespread use [14].

The heat transfer through windows is characterized by very complex physical phenomena leading to variations heat flux density across different parts of the window. This experimental research aims to determine the heatflux densities on the lower, central, and upper parts of external surfaces of triple-pane windows within a climatic chamber. The study compares heat flux density distributions, *U*-values, and *R*-values of both air- and argon-filled windows, considering the use of low-emissivity coatings and electric heating.

Materials and Methods

Materials

The experimental study was conductedat the Laboratory of Material Structure and Heat Exchange at the Kielce University of Technology (Poland), using a climatic chamber. The climatic chamber consists of two boxes: an internal (hot) box *measuring 2.25 m x 1.8 m x 2.30 m,* simulating indoor conditions *with adjustable temperatures ranging from +5℃ to +50℃, and an* external (cold) box *measuring 2.70 m x 1.80 m x 2.30 m*, simulating outdoor conditions *with adjustable temperatures ranging from -25℃ to +80℃*. The internal box is movable, allowing for the assembly of the tested building partitions between the two boxes. Figure 1 provides a general view of the climatic chamber at the Kielce University of Technology.

FIGURE 1. *General view of the climatic chamber at the Kielce University of Technology*

The system under investigation comprised four triple-pane windows adapted to be installed in a climatic chamber. Each window had a height of 87.5 cm and a length of 60.0 cm. The windows were mounted in a reinforced concrete wall using an aluminum frame (warm profile). The reinforced concrete wall was positioned between the cold and hot parts of the climatic chamber and was thermally insulated with a 20 cm layer of mineral wool on the cold side. A photograph of the experimental setup is presented in Figure 2.

FIGURE 2. *Photograph of the climatic chamber testing plane*

Figure 3 illustrates the cross-sectional diagrams of the tested triple-pane windows.

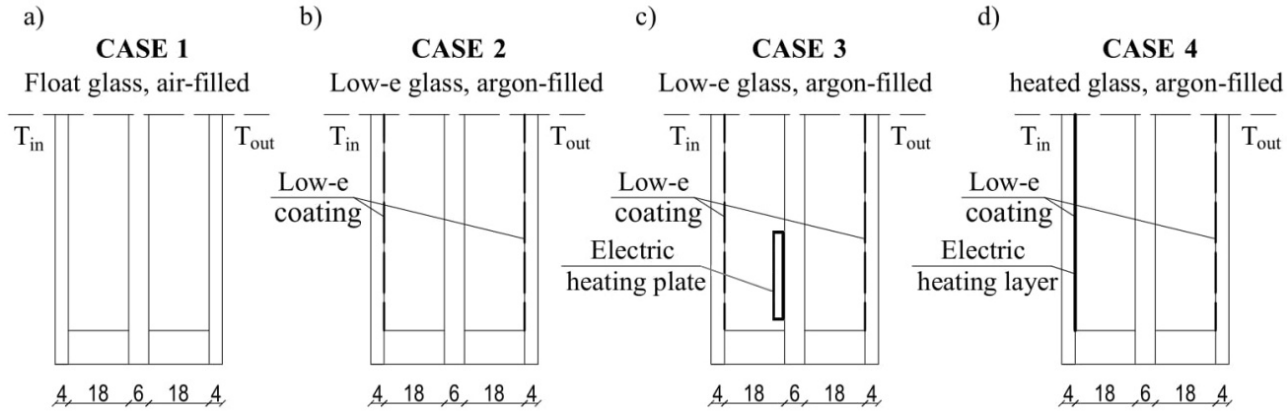

FIGURE 3. *Cross-sectional diagrams of the tested triple-pane windows*

As depicted in Figure 3, each outer and inner pane had a thickness (t) of 4 mm, while each central pane had a thickness of 6 mm. The width of the gaps between the panes was 18 mm. In Case 1 (Fig. 2a), the window consisted of three float glass panes with emissivity (ε) of 0.84 and thermal conductivity (k) of 0.92 W/mK, separated by air-filled gaps. Case 2 (Fig. 2b) examined the use of inert gas (argon) filling and low-emissivity coatings (ε = 0.17) on the inner pane surface facing the gap. Case 3 (Fig. 2c) involved the installation of an electric heating plate in the lower part of the room-side gap, on the central pane, comprising resistance rods with a resistance of 50 Ω. The power supply wire, suitable for plugging into a 230 V socket, was routed from the inner side of the window frame. In Case 4 (Fig. 2d), the window operated by combining electric current with a low-emissivity metal oxide layer on the inner pane surface facing the gap. The power supply wire was connected to a thermostat that controlled the window's temperature.

Apparatus

The FHF04 foil heat flux sensor (Hukseflux) with **sensitivity** of Φ_i = 10.48 μV/(W/m²) was attached to the lower, central and upper parts of the outer pane surface to monitor the heat flux density distribution of each window. The red dots in Figure 4 represent the sensor locations.

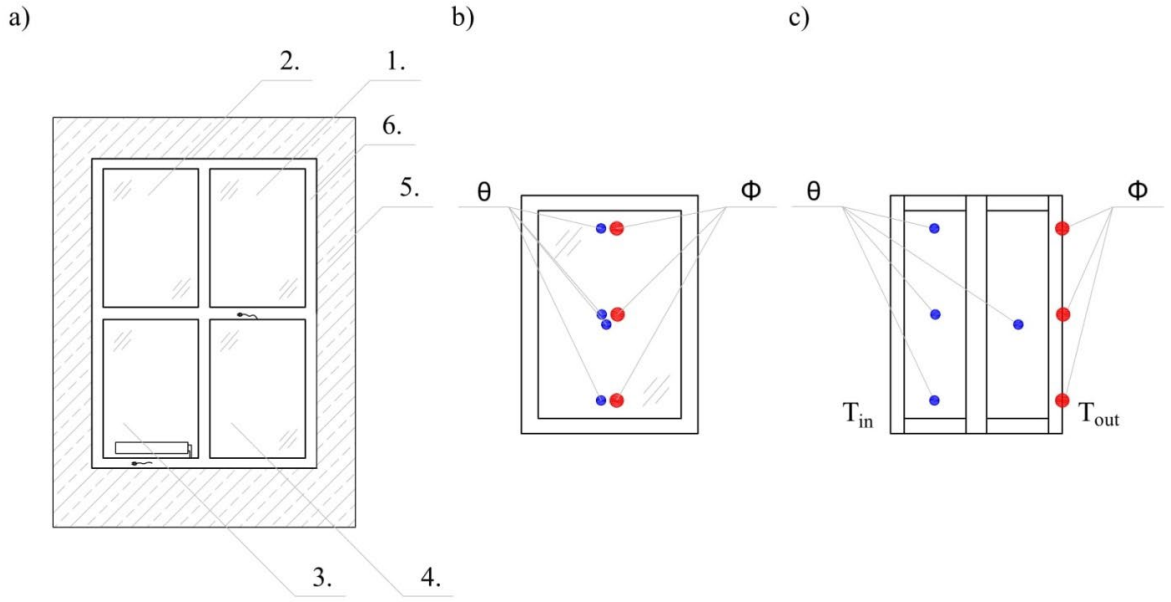

FIGURE 4. *Cross-sectional diagrams of the tested triple-pane windows: 1, 2, 3, 4 – tested windows (case 1 to 4); 5 – reinforced concrete wall; 6 – aluminium frame; Φ – heat flux meters; θ – thermocouples; T_{in} – indoor box ambient, T_{out} – outdoor box ambient*

The FHF04 sensors measured heat flux from conduction, radiation, and convection. Moreover, three K-type thermocouples were placed within the lower, central, and upper parts of the internal gap, and one K-type thermocouple was installed in the central part of the external gap in order to measure the cross-sectional temperature levels of each window. The blue dots in Figure 4 represent the thermocouple positions. The LI19 heat flux density data-logger (Hukseflux) was used to display and store the minimum, maximum and average heat flux measurements, along with corresponding date and time.

Additionally, the digital TM-947SD four-channels thermometer with data-logger (Lutron) was employed to record the temperature of the gas layer between the panes using K-type thermocouples. The Testo 872s thermal imager was utilized to capture thermal images for further analysis. Table 1 provides a summary of the apparatus employed in the experimental measurements.

Table 1. *The apparatus used in the experimental measurements*

Instrument	Measurement	Sensitivity	Range
K-type thermocouples	temperature	41 μV/°C	−100°C to +400°C
Foil heat flux sensors (FHF04, Hukseflux)	heat flux	10.48 μV/W/m^2	(−10 to +10) x 10^3 W/m^2
Thermometer with data-logger (TM-947SD)	average temperature	–	–
Heat flux density data-logger (LI19, Hukseflux)	minimum, maximum and average heat flux	–	–
Thermal imager (Testo 872s)	thermography	0.05°C	-30°C to +100°C; 0°C to +650°C

Methods

The experimental study was conducted within the climatic chamber under constant conditions of an air temperature of 20°C in the hot box and a humidity level of 50%. In order to demonstrate the effect of external temperature on heat flux through the windows, tests were carried out at three different cold box temperatures: -5°C, 0°C and +5°C. The measurements were taken once both chambers reached a steady state, with the air temperature remaining constant and varying within 2% per hour. The tests continuously recorded results at 2-second intervals over a period of 1 hour. All measurements were conducted following the guidelines outlined in ISO 9869-1:2014.

The thermal transmittance (U) was calculated by dividing the average heat flux density on each part of the external glazing by the average temperature difference between the interior and exterior panes surfaces, as shown in equation (1) [15]. The thermal resistance (R) was calculated using equation (2) [15]

$$U = \frac{\sum_{j=1}^{n} q_j}{\sum_{j=1}^{n} \left(T_{sij} - T_{sej} \right)}, \frac{\mathrm{W}}{\mathrm{m^2K}} \tag{1}$$

$$R = \frac{\sum_{j=1}^{n} \left(T_{sij} - T_{sej} \right)}{\sum_{j=1}^{n} q_j}, \frac{\mathrm{m^2K}}{\mathrm{W}} \tag{2}$$

where:

U – thermal transmittance, W/m^{2}K;
R – thermal resistance, m^{2}K/W;
q – heat flux density, W/m^2;

T_{sij} – internal glazing surface temperature, °C;

T_{sej} – external glazing surface temperature, °C.

However, it is important to note that this test has certain limitations. Unfortunately, the climatic chamber used in this study is not equipped to investigate the impact of solar radiation. Consequently, thethermal performance of windows in the presence of solar radiationis not addressed in this study. Therefore, the results presented here should be considered comparable to reports with similar methodologies. Future research focusing on the influence of solar radiation on heat flux density distribution would be an interesting avenue to explore.

Results and discussion

The results of the experimental study are presented in both graphical and tabular formats. Figures 5-8 display the average heat flux density recorded on the lower, central and upper parts of external glazing of each window at an outside temperature of T_{out} = -5°C. Additionally, Figure 9 shows athermal image of Case 1, captured from the warm box side. The comparison between measurements and calculations is summarized in Table 2.

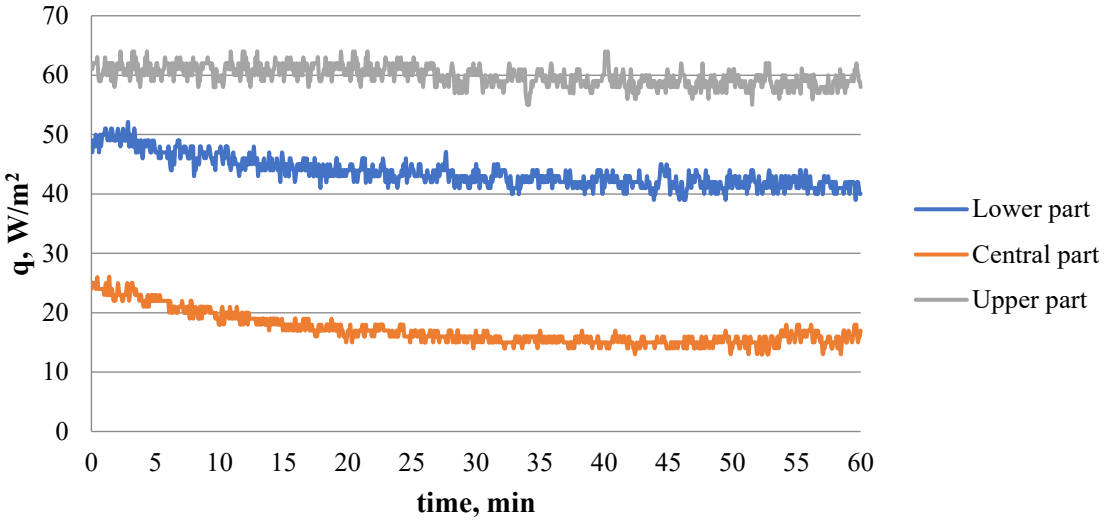

FIGURE 5. *Average heat flux density values on the external glazing for the lower, central, and upper parts of the window in Case 1 (T_{out} = -5 ℃)*

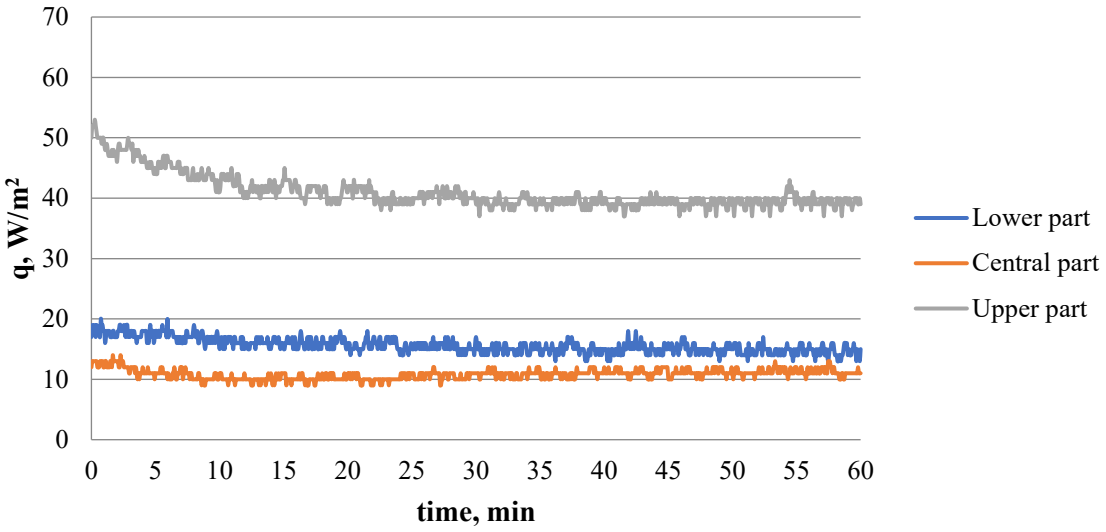

FIGURE 6. *Average heat flux density values on the external glazing for the lower, central, and upper parts of the window in Case 2 (T_{out} = -5 ℃)*

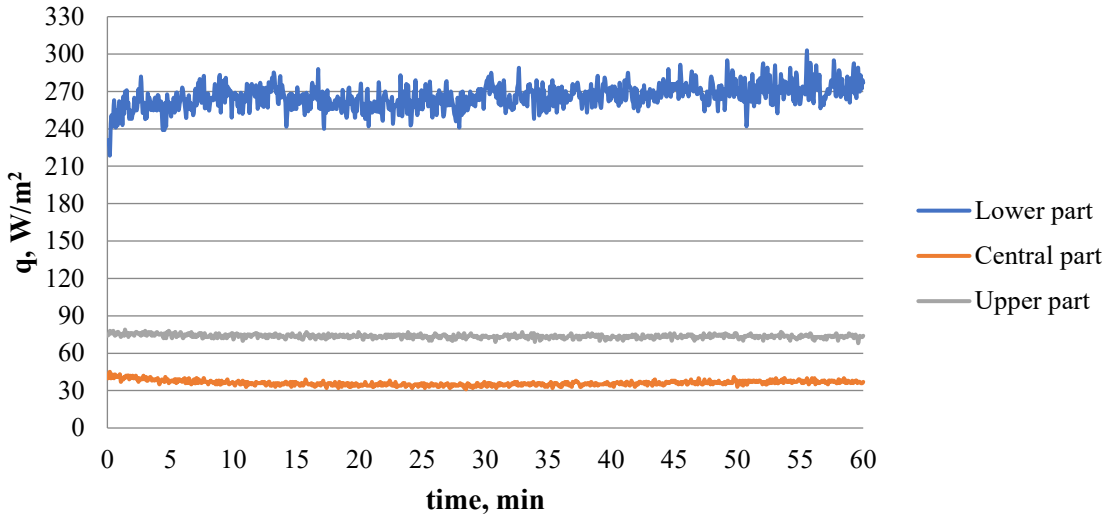

FIGURE 7. *Average heat flux density values on the external glazing for the lower, central, and upper parts of the window in Case 3 (T_{out} = -5 ℃)*

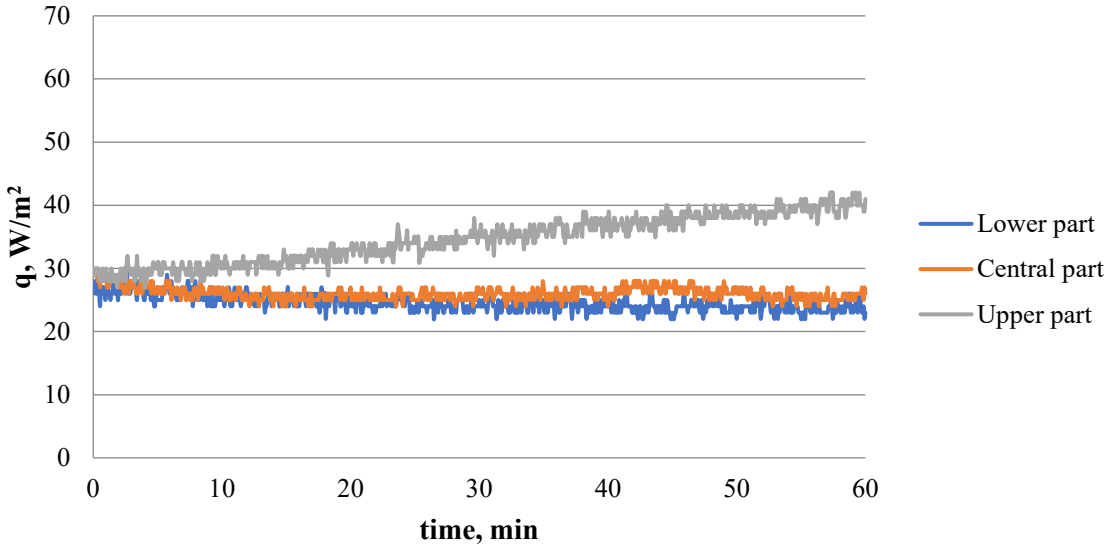

FIGURE 8. *Average heat flux density values on the external glazing for the lower, central, and upper parts of the window in Case 4 (T_{out} = -5 ℃)*

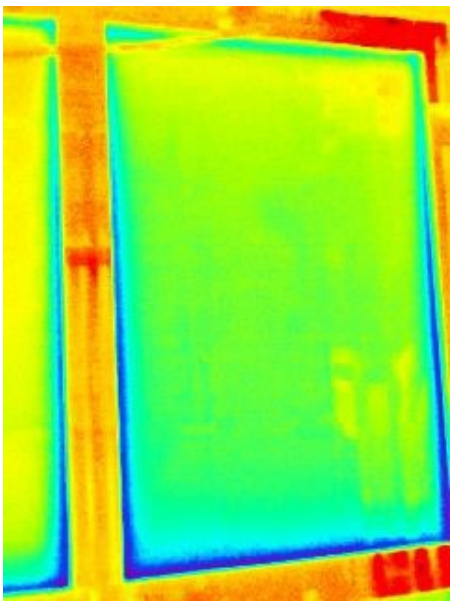

FIGURE 9. *Thermal image of Case 1captured from the warm box side*

Table 2. *Comparison of the measured average heat flux density and the calculated thermal transmittance and thermal resistance*

	Part	Case 1	Case 2	Case 3	Case 4
q, W/m^2	lower	43.6	15.6	265.7	24.6
	central	18.0	10.8	36.1	26.0
	upper	59.8	41.0	73.7	34.6
U-value, W/m^{2}K	lower	2.422	0.918	9.194	1.166
	central	1.000	0.647	1.327	1.182
	upper	3.322	2.515	2.632	1.747
R-value, m^{2}K/W	lower	0.413	1.090	0.109	0.858
	central	1.000	1.546	0.753	0.846
	upper	0.301	0.398	0.380	0.572

Conclusions

This study investigated the heat flux densitydistribution in triple-pane windows filled with airand argon, considering the use of low-emissivity coatings and electric heating. Experimetal analysis was conducted, and the results presented in Figures 5-8 indicated that heat flux densities remained relatively stable over time under constant outdoor temperature conditions without solar radiation. The variation in heat flux density across different parts of the glazing surface was primarily influenced by convection within the gas-filled gap between the panes and the differing thermal properties of the materialsused (glass, spacer, and window frame). Based on the obtained results, the following conclusions can be drawn:

1. Steady-state conditions revealed significant discrepanciesin heat flux density acrossdifferent parts of the external glazing of each window, attributed to convective multicellular circulations within the gas layer.
2. The hermal transmittance varied among the lower, central, and upper parts of the external glazing of each window due to the disctinct conductive properties of window materials and convection effects near the glazing and windows edges.
3. For the air-filled triple-pane window with float glass panes (Case 1), the highestheat flux density value of 64 W/m^2 was observedon the upper part of the external glazing, while the lowest value of 14 W/m^2 was measured on the central part. This resulted in U-values that were more than 2 and 3 times higher in the lower and upper parts, respectively, compared to the central part.
4. The argon-filled window with low-emissivity coating (Case 2) exhibited a 35% reduction in heat flux density on the central part compared to the air-filled window (Case 1). The U-values were determined as 0.918, 0.647, and 2.515 W/m^2·K for the lower, central, and upper parts, respectively (Case 2).
5. The use of local electric heating in the lower part of the central paneproved to be ineffective, resulting in an increase in heat flux density through the bottom of the window by over 17 times compared to Case 2. This led to the poorest thermal resistance among all tested windows.
6. Surface electric heating (Case 4) resulted in a more uniform distribution of heat flux densities along the height of the outer pane, with values of 24.6, 26.0 and 34.6 W/m^2 for the lower, central and upper parts, respectively. The thermal resistance values along the entire height of the window were the most consistentamong the tested windows.
7. These findings emphasize the importance of considering the variability of thermal resistance across the entire height of windows. Therefore, considering this variability is crucial for an accurate calculation of the heat transfer coefficient.

References

[1] Cuce E., Riffat S.B., *A state-of-the-art review on innovative glazing technologies.* Renewable and Sustainable Energy Reviews 2015, 41, 695-714, https://doi.org/10.1016/j.rser.2014.08.084.

[2] Basok B.I., Davydenko B.V., Isaev S.A., Goncharuk S.M., Kuzhel L.N., *Numerical modeling of heat transfer through a triple-pane window*, Journal of Engineering Physics and Thermophysics 2016, 89(5), 1277-1283, https://doi.org/10.1007/s10891-016-1492-7.

[3] Basok B., Davydenko B., Novikov V.G., Pavlenko A.M, Novitska M.P., Sadko K., Goncharuk S.M., *Evaluation of heat transfer rates through transparent dividing structures*. Energies 2022, 15, 4910, https://doi.org/10.3390/en15134910.

[4] Nia M.F., Nassab S.A.G., Ansari A.B., *Transient numerical simulation of multiple pane windows filling with radiating gas*, International Communications in Heat and Mass Transfer 2019, 108, 104291, https://doi.org/10.1016/j.icheatmasstransfer.2019.104291.

[5] Basok B., Davydenko B., Zhelykh V., Goncharuk S., Kuzhel L., *Influence of low-emissivity coating on heat transfer through the double-glazing windows*, Building physics in theory and practice (Fizyka budowli w teorii i praktyce) 2016, 8(4), 5-8.

[6] Arıcı M., Kan M., *An investigation of flow and conjugate heat transfer in multiple pane windows with respect to gap width, emissivity and gas filling*. Renewable Energy 2015, 75, 249-256, https://doi.org/10.1016/j.renene.2014.10.004.

[7] Rojewska-Warchał M., *The influence of glazing type, frame profiles, shape and size of the window of the final value of window thermal transmittance U*. Czasopismo Techniczne, Architektura 2014, 8A(15), 199-206, https://doi.org/10.4467/2353737XCT.14.206.3294.

[8] Arıcı M., Karabay H., Kan M., *Flow and heat transfer in double, triple and quadruple pane windows*. Energy and Buildings 2015, 86, 394-402, https://doi.org/10.1016/j.enbuild.2014.10.043.

[9] Aguilar-Santana J.L., Velasco-Carrasco M., Riffat S., *Thermal Transmittance (U-value) Evaluation of Innovative Window Technologies.* Future Cities and Environment 2020, 6(1). http://doi.org/10.5334/fce.99.

[10] Cuce E., *Accurate and reliable U-value assessment of argon-filled double glazed windows: A numerical and experimental investigation.* Energy and Buildings 2018, 171, 100-106, https://doi.org/10.1016/j.enbuild.2018.04.036.

[11] Pavlenko A.M., Sadko K., E*valuation of Numerical Methods for Predicting the Energy Performance of Windows.* Energies 2023, 16, 1425, https://doi.org/10.3390/en16031425.

[12] Lee R., Kang E., Lee H., Yoon J., *Heat Flux and Thermal Characteristics of Electrically Heated Windows: A Case Study.* Sustainability 2022, 14, 481, https://doi.org/10.3390/su14010481.

[13] Gloriant F., Joulin A., Tittelein P., Lassue S., *Using heat flux sensors for a contribution to experimental analysis of heat transfers on a triple-glazed supply-air window*. Energy 2021, 215(A), 119154, https://doi.org/10.1016/j.energy.2020.119154.

[14] Gori V., Marincioni V., Biddulph P., Elwell C.A., *Inferring the thermal resistance and effective thermal mass distribution of a wall from in situ measurements to characterise heat transfer at both the interior and exterior surfaces*. Energy and Buildings 2017, 135, 398-409, https://doi.org/10.1016/j.enbuild.2016.10.043.

[15] BSI. 2014. ISO 9869-1:2014 – Thermal insulation — Building elements — Insitu measurement of thermal resistance and thermal transmittance; Part 1: Heat flow meter method.

Paweł LESIAK

Faculty of Environmental Engineering, Geodesy and Renewable Energy,
Kielce University of Technology, Kielce, Poland
al. Tysiąclecia Państwa Polskiego 7, 25-314, Kielce, Poland

Corresponding author: plesiak@tu.kielce.pl

Doi: 10.53412/jntes-2023-2-4

ZEOLITES AS CATALYSTS: A REVIEW OF THE RECENT DEVELOPMENTS

Abstract: *The article presents the latest solutions (period 2015-2023) regarding zeolites and zeolitic materials used as catalysts for chemical reactions. The use of zeolites, among others, was presented and discussed for the purification of gases and sewage, as a raw material for the production of cement, as a component of dressings for hard-to-heal wounds, for blood purification, for the purpose of controlled release of drugs, as molecular sieves, or for the protection of monuments. The use of zeolites as catalysts and the trends in their use for this purpose are discussed with particular emphasis.*

Keywords: *zeolite, application, biomass conversion, biofuels production, pyrolisis procceses, water purification procceses*

Introduction

The first zeolite was discovered in the 18th century, when it was noticed that the mineral stilbite began to release significant amounts of water vapor when heated. This led to the understanding that water could be adsorbed on the surface of the material. Further research has identified many minerals of the zeolite family with many different structural configurations and pore sizes. There are about 70 types of natural zeolites, and more than 260 synthetic zeolites are registered [1]. The most common forms are clinoptilolite, mordenite, phillipsite, chabazite, stilbite, and laumontite, while offretite, paulingite, barrerite and mazite are not very common. Among them, clinoptilolite is the most abundant natural zeolite in nature and is widely used around the world.

Zeolites have found their application in many different fields. One of them is, for example, air-conditioning systems, filtration of drinking water, water and sewage treatment – mainly clinoptilolite filters are used there, which purify water from coarse suspensions and colloidal particles of mineral and organic origin. In combination with chlorination, ozonation and contact coagulation, drinking water is effectively purified. Another use is pool filters. Zeolites can also be used to deactivate radioactive wastewater by adsorption deactivation [1]. The ion-exchange selectivity of clinoptilolite towards cesium, strontium and other radioactive elements greatly facilitates this task. Zeolites also support groundwater treatment plants from radioactive isotopes and heavy metals. They are used during aeration of aquatic organisms with oxygen obtained by air separation. They absorb unpleasant odors and moisture, which is why they are a component of bedding for animal litter boxes. Zeolites were also used to deactivate nuclear waste after the Chernobyl nuclear power plant disaster. It is also worth mentioning that they are used to make very effective heat exchangers used in the power industry [2]. All this indicates a growing interest in zeolites and new innovative ideas for their use.

The purpose of this text is to present, on the basis of examples, the solutions studied in recent years and what the trends look like and what challenges they must meet.

Application of zeolite today

Taking into account all the properties of zeolites, the possibilities of its use are very wide. They are shown in Figure 1.

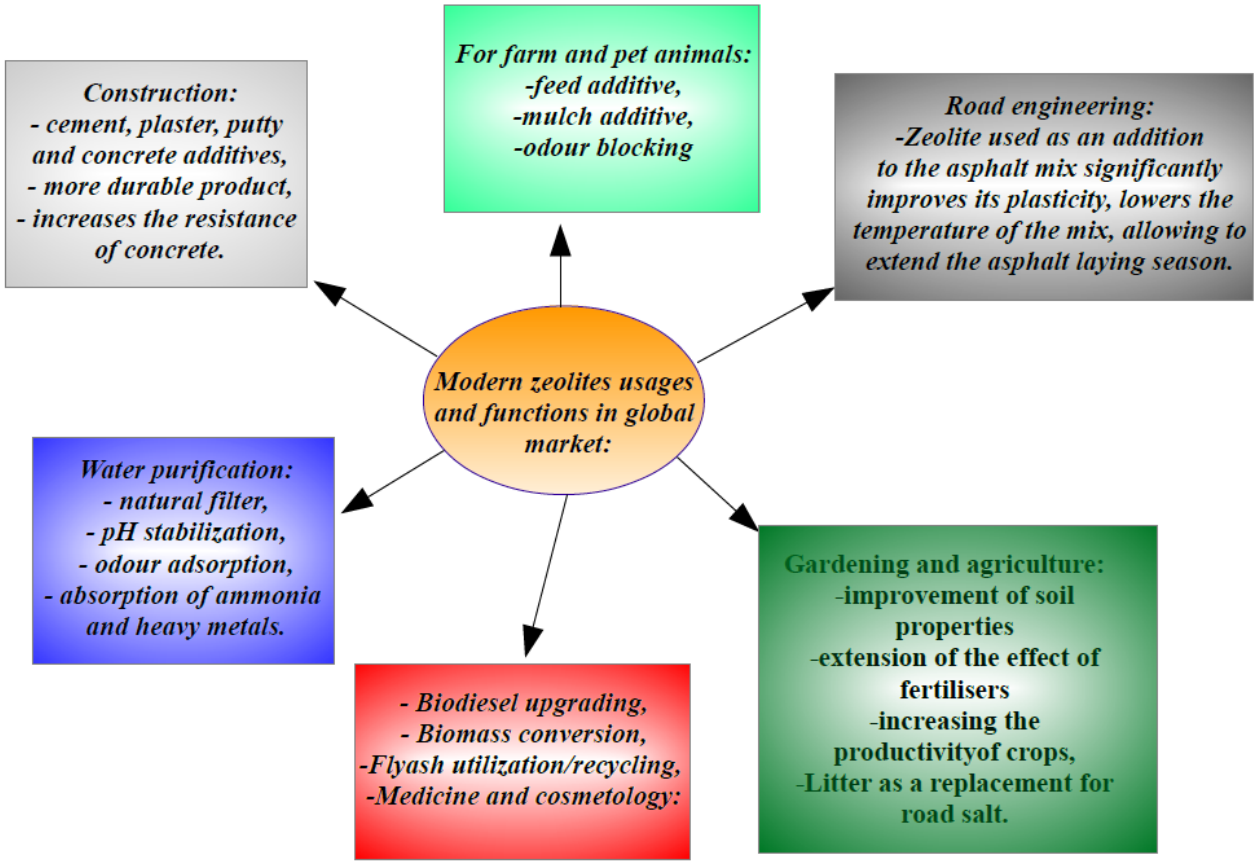

FIGURE 1. *Modern zeolite usage and various functions in global market*

There are several ways to increase the use of zeolites. The most commonly used zeolite modification techniques include:

- ion exchange in the liquid phase,
- solid phase ion exchange,
- impregnation with salts of metal precursors,
- dealumination,
- incorporation of metals into the structure of the zeolite,
- desilatation,
- deposition of active material from the gas phase [3, 4].

According to economic analyses, the market of zeolites is growing year by year, which shows. Figure 2 with assumed economic projections from 8.5 billion USD for 2022 to even 12.7 billion USD in 2032.

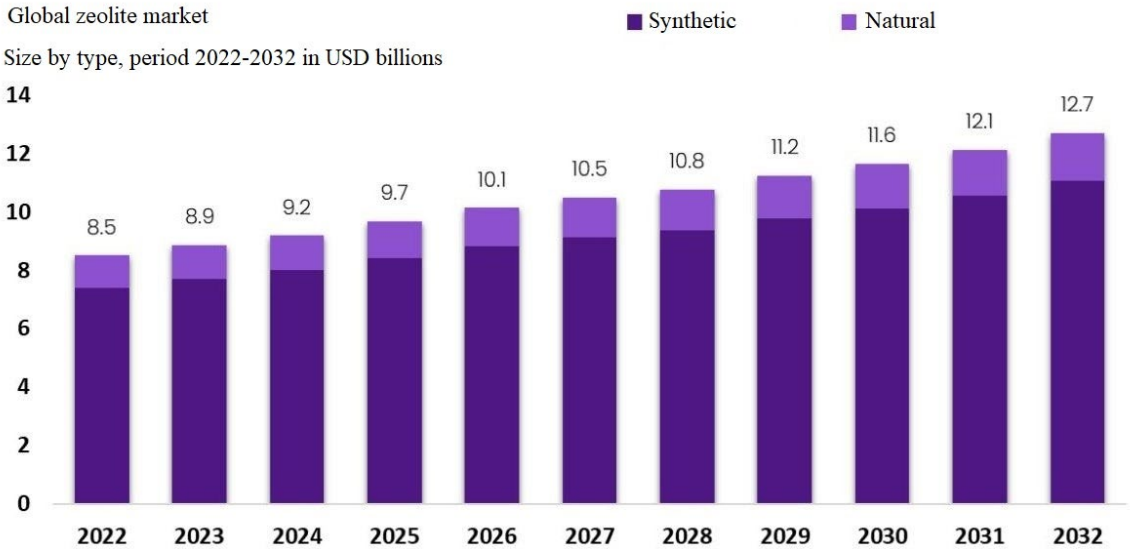

FIGURE 2. *Global zeolite forecast of market size from 2022 to 2032 [5]*

As can be seen in Figure 3, the largest market for zeolites, having nearly half of the total value from 2022, are catalysts. Another over 30% of the value are adsorbents and detergent additives. The use of zeolites for the production of cement, animal feed and other purposes accounts for about 20% of the market. It can be easily assumed that in the future, further and new applications will constitute an increasing proportion of the global market for the trade and production of zeolites.

Examples of modern usage of zeolites in biomass conversion

In response to the growing demand for fossil fuels, the rising cost of production and environmental concerns, the valorization of cheap, widely available and renewable biomass from waste is very beneficial for industrial applications using a zeolite-based catalysis reaction. The amount and variety of biomass waste currently available offers the opportunity to produce industrially useful chemicals and valuable commodities. Such zeolites can be used in various industrial sectors, such as the chemical, pharmaceutical, cosmetic and food sectors. One of the many applications in which the greatest hopes are currently pinned is the synthesis of biogas, which is a promising alternative fuel with low CO_2 emissions and high market potential due to the abundance of organic biomass. Biogas, despite being a renewable form of energy, usually contains 40-45% CO_2, which significantly reduces its calorific value. Many porous materials have been adapted to adsorb gaseous CO_2 from the biogas stream in order to obtain biogas with a biomethane content of 95-97%. Zeolites are therefore one of the promising porous materials that can significantly contribute to the upgrading process through selective adsorption of gaseous CO_2 from biogas [6]. The use of natural material as a catalyst or a substrate for the production of a catalyst not only reduces the costs associated with the production of catalysts, but also makes the process used environmentally friendly. In addition, the use of waste materials reduces the problem of waste disposal. The most abundant by-products of technology include, above all, waste from agriculture, mining and metal production, in particular from the steel industry [7].

In recent years, the use of zeolites in biomass conversion processes has developed significantly [8]. More precise biomass component conversion technologies are gradually replacing traditional biomass cracking processes, comparable to today's oil-based petrochemical industrial activities. As a consequence, lignocellulosic biomass can be transformed into a sustainable feedstock for the production of bulk chemicals and fuels in the coming years. Zeolites have the potential to be used in these types of processes, and their availability and adaptability make them a fascinating prospect to explore. In previous years, several new possibilities for the selective production of zeolite particles were discovered, which are now being studied in great detail, which is also necessary to reduce the overall environmental impact of the chemical industry.

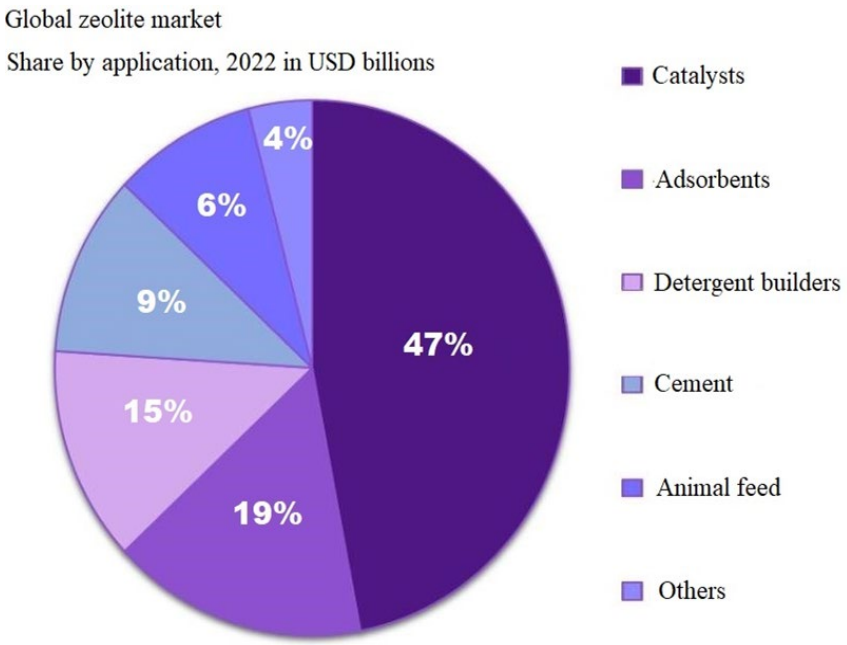

FIGURE 3. *Global zeolite market divided into biggest usages [5]*

Another popular waste in the transformation of which zeolites can help is fly ash and its use as a substrate for the synthesis of zeolites. Then its transport and storage in appropriate geological structures or mineral sequestration [9]. As it results from the research presented in [10], activation with silver by ion exchange method allows to obtain a zeolite form of the Ag-X type. On the other hand, activation with silver (Ag-X) allowed to obtain more than five times longer time to breakthrough (5% wt. and 10% wt. HgO) compared to the commercially available bromine-modified activated carbon (AC/Br). Determination of the sorption capacity showed that activation with silver did not significantly affect the sorption properties of the zeolite towards CO_2. The results of sorption in dynamic conditions indicate the possibility of using the Ag-X zeolite as a sorbent for gaseous forms of mercury [11].

Examples of zeolites usage in biofuels production

One of the most innovative solutions, presented by the authors of paper [12], is the conversion of oil from the larvae of the Black Soldier Fly (BSF – Black Soldier Fly lat. Hermetia illucens) into hydroxysodalite zeolite (HS) synthesized from waste coal of fly ash (CFA) in the production of biodiesel. The zeolite product obtained after CFA fusion followed by hydrothermal synthesis (F-HS) gave a highly crystalline, mesoporous F-HS zeolite with a significant surface area of 45 m^2/g. The parent F-HS zeolite catalyst gave a high biodiesel yield of 84.10% with good quality and 65% fatty acid methyl ester (FAME) fuel characteristics meeting standard biodiesel specifications. The F-HS zeolite derived from CFA waste showed favorable performance as a heterogeneous catalyst compared to the conventional sodium hydroxide (NaOH) homogeneous catalyst. The zeolite catalyst provided a more cost-effective process using BSF fly oil and was economically comparable to NaOH for every kilogram of biodiesel produced. In addition, this study showed the potential to address the general cost challenge of biodiesel production by developing waste-derived catalysts and BSF worm oil as low-cost alternative feedstocks.

In another case, the catalytic conversion of CO_2 with a surplus of glycerol (GL) produced during the production of biodiesel has attracted much academic and industrial attention, demonstrating the urgent need to develop high-performance catalysts with significant environmental benefits. In studies [13], catalysts based on ETS-10 zeolite with titanium tanosilicate with active metals introduced by impregnation were used to couple CO_2 with GL for the efficient synthesis of glycerol carbonate (GC). The catalytic conversion of GL at 170°C reached 35.0% and a 12.7% higher yield of GC to Co/ETS-10 was obtained with CH_3CN as a dehydrating agent.

Examples of conversion of Fly Ash waste into zeolites

As a result of thermal treatment of waste in incineration plants, large amounts of ashes and slags are generated, which contain significant amounts of heavy metals, dioxins and furans [14]. The issue of such secondary waste has recently gained importance due to the construction of new waste incineration plants in Poland. Such materials should be properly processed and managed. One of the possibilities of using post-process waste from waste incineration plants is the technology of producing zeolites and sorbents. The manufactured products have ion exchange capabilities and can be used in a number of applications. Based on research [15], the following conclusions were formulated:

1. The usefulness of selected post-process waste from the waste incineration plant for the production of zeolites in hydrothermal alkaline activation processes was found.
2. The synthesis of ashes and slags from waste incineration plants in an alkaline environment leads to a change in the morphology of these ashes. One of the mineral components of the synthesis products are zeolites - e.g. Sodalite.
3. In order to improve the efficiency of obtaining zeolites from slags, it is necessary to crush/grind tchem.
4. It is also necessary to carry out detailed studies of pore size and surface area.

Disposal of Municipal Waste Fly Ash (MSWFA) remains a challenging task. Unlike coal fly ash (CFA), which can be used for the synthesis of various types of zeolite-like materials, MSWFA is devoid of silicon and aluminum, which are necessary for the synthesis of zeolites. According to a study by [16] using MSWFA by silicon and aluminum source addition method from various solid wastes to achieve recycling utilization, that the products obtained by both hydrothermal and fusion treatment showed zeolite-like material properties. Compared to the raw materials, the synthetic products showed a higher cation exchange capacity of 1.00 meq/g, suggesting application potential by converting MSWFA into usable materials.

Another solution presented by the authors of paper [17] are fly ash-based geopolymers as stable bifunctional heterogeneous catalysts in Friedel-Crafts acylation reactions. Class C coal fly ash was used as a precursor to reactive, inexpensive and environmentally friendly heterogeneous catalysts based on geopolymers. The developed catalysts showed high reactivity with excellent selectivity towards very demanding Friedel-Crafts acylation of various surfaces. The high reactivity of geopolymer-based catalysts is attributed to the different active sites they possess; Lewis and Brønsted acid sites that are generated within them and the catalytically active Fe_2O_3 compounds present in the original fly ash. This combination of different sites is expected to provide bifunctionality in the catalysis of acid and/or redox catalysed reactions. The metal oxide particles are either encapsulated in the geopolymer matrix or glued to the geopolymer particles, therefore these catalysts are expected to have a high degree of reusability and catalyst lifetime.

According to [18], zeolite, which was synthesized from three different types of waste (i.e. fly ash, sludge and contaminated soil), was then used as a carrier for the preparation of a catalyst for the hydrogenation of nickel to levulinic acid and γ-valerolactone. Under optimal synthesis conditions, the newly synthesized geopolymer zeolite has excellent structure and performance. The characterization results indicate that the composites have a three-dimensional network structure, and the pore structure is homogeneous, mesoporous or microporous. In [19], the results of catalytic hydrogenation show that the yield of γ-valerolactone can reach 94% using the synthesized catalyst, which is comparable to the yield of commercial catalysts and the concentrations of typical contaminating heavy metals Cu, Zn, Pb and Cd in the reaction solution were below the concentration limit emissions (class I standard) after five reaction cycles. In conclusion, the geopolymer type catalyst is cheap and has excellent performance; therefore, it is expected to be widely used in catalysis instead of commercial supports. The authors [20] in their work expect that in the future this material will also be used in various high-value fields, such as electrocatalysis and adsorption.

Examples of zeolites usage in pyrolisis procceses

Bio-waste valorisation is an excellent way to deal with resource depletion and climate change, with benefits for the environment and economic growth. One of the best-known technological ways of converting bio-waste into bio-products is pyrolysis, which is gaining more and more importance as a technology used for the production of alternative fuels and chemicals. This reaction may be carried out using a catalyst.

One of the materials that can support the production of synthetic zeolites considered recently is the pyrolysis of MPFP (Multi-layered Plastic Food Packaging) waste, widely used in food production, which is currently difficult to recycle due to the variety of materials from which individual layers of packaging are made and often it is incinerated instead of being reused [21]. The same applies to plastic waste from scrapped cars, which is mostly not reused. The authors of the paper [22] analyzed the catalytic pyrolysis of a realistic mixture of MPFP multilayer waste, such as plastic food packaging and ZSM-5 zeolite synthesized from them, for the pyrolysis reaction and obtaining final products such as oil and gas. An example of the tested MPFP waste mixture contained 71.9% PET, 25.1% PE and 3.0% PP. Each sample was cut into small pieces of 2-3 mm. The metallization of the film was carried out using a plasma metallization process, resulting in very fine particles that could not be measured in μm. The thermal behavior, kinetic parameters and pyrolysis kinetic model of multi-layer plastic food packaging were determined to show the potential of the process at scale. These experiments used a powdered ZSM-5 zeolite catalyst defined by the MFI crystal structure and loaded with iron(III) oxide. The main characteristics of the catalyst are a pore diameter ranging from 2.5 to 5 nm, a specific surface area of 135 $m^2\ g^{-1}$, an average particle size of 82 μm and a SiO_2/Al_2O_3 ratio of 4.07. Thermal decomposition occurred in the range of 350-510°C, with a weight loss of more than 90%. The kinetic study revealed a complex pyrolysis process that consisted of three stages of decomposition, diffusion and Avrami-Erofeev type reaction. The activation energy values determined by the Friedman method increased with the degree of conversion from 127 kJ mol^{-1} at 0.01 to 219 kJ mol^{-1} at 0.95. Catalyst doping lowered the activation energy of the reaction by 44% and 8%, respectively, in the first and second stages, and increased the acidity of the zeolites, thereby increasing the reactivity on the surface of the catalysts. The lower activation energy meant that less energy was required to heat the pyrolysis reactor as the sample's onset temperature was lowered and the ZSM-5 synthetic zeolite was found to be effective in its intended role.

Catalytic pyrolysis of plastic waste using zeolites produced from fly ashes from coal was the subject of work [23]. Residual PFR film was selected as the raw material for pyrolysis. The authors conducted thermal and catalytic pyrolysis experiments, and coal fly ash (CFA) and X zeolite synthesized from CFA (X/CFA) were used as pyrolysis catalysts. The main goal is to study the effect of cheap catalysts on the efficiency and quality of pyrolysis oils. The fusion/hydrothermic NaX/CFA was ion exchanged and then calcined to produce HX/CFA. First, thermogravimetry and differential scanning calorimetry (TG and DSC, respectively). The analyzes performed assessed the effect of catalysts on the PFR degradation temperature and on the energy demand of the process. The pyrolysis run showed that the highest oil yield (44 wt%) was obtained by HX/CFA, while the main products obtained by thermal pyrolysis were wax and tar. In addition, up to 70% of the HX/CFA oil consisted of gasoline-range hydrocarbons. The gases produced had a combustion energy up to 8 times higher than the energy needed for pyrolysis.

Examples of zeolites usage in water purification procceses

Clinoptilolite is one of the most widespread and naturally occurring zeolites. Its availability, low cost, and unique ion-exchange properties make it an excellent candidate for both direct application and various modifications to create new low-cost functional materials for sustainable development. Specific applications where clinoptilolite is already used include water treatment and removal of heavy metal ions, agricultural purposes, storage and conversion of unwanted gaseous emissions to the atmosphere, production of catalysts and photocatalysts, bioactive materials and many others [24]. However, unlike some other zeolites, clinoptilolite is difficult to synthesize [25], therefore most publications refer to this

zeolite in its natural form, either directly from the deposit or after various processes have been applied to improve its properties. Among the modification methods used, ion exchange stands out the most.

Studies presented by [26] on zeolite for removing trace metal ions from water showed that natural zeolite in the form of clinoptilolite derived from tuffs can be used as a material for removing heavy metal ions from groundwater in the technology of permeable active barrier. The highest efficiency of removing zinc and cadmium ions (>90%) was obtained at pH = 6÷7 and their initial content in the range of 5÷25 g/m^3. This also confirmed the good efficiency of zeolite as an active material for removing zinc and cadmium ions from water with a slightly acidic pH and not very high (approx. 25 g/m^3) initial amounts of these impurities. The effective action of the zeolite (approx. 99%) was maintained for a time corresponding to 5-6 times the exchange of the volume of the zeolite bed as a permeable active barrier. The author [2] demonstrated the effectiveness of removing both zinc and other metals present in wastewater. For sewage with a zinc concentration of 130 mg/dm^3, in order to reduce the zinc concentration to the standard level of 2 mg/dm^3, it was necessary to dose zeolite in the amount of 50 g/dm^3. It was shown that the use of synthetic zeolites made it possible to obtain concentrations below the normative values for all metals present in the tested wastewater.

Conclusions

Zeolites are an excellent response to the market demand for natural and ecological materials, the use of which can have a real and conscious impact on the condition of the natural environment. As the analysis of the market of zeolites shows, their use is constantly increasing and forecasts predict an annual increase in the value of the zeolite market. As the presented analysis shows, zeolites are materials with almost unlimited applications in many fields, such as industry and environmental protection.

The review of the latest trends and applications presented in the article shows the great importance of the use of zeolites for such purposes as catalysis, biomass conversion, biofuel production and refining, fly ash recycling, hydrogenation of metals to acids or various wastewater treatment methods shows how versatile these minerals are. One of the most important problems was the production of an efficient catalyst for wastewater treatment, which is constantly being developed. The issue of reducing emissions and taking greater care of the natural environment additionally promotes the use of such innovative methods. Nowadays, they can be a cheap alternative to known and energy-intensive technologies known for a long time. The fact that zeolites are constantly developed and modified proves their great potential in many branches of the economy.

References

[1] Morante-Carballo F., Montalván-Burbano N., Carrión-Mero P., Espinoza-Santos N., *Cation Exchange of Natural Zeolites: Worldwide Research.* Sustainability 2021, 13(14), 7751, https://doi.org/10.3390/su13147751; https://www.mdpi.com/2071-1050/13/14/7751.

[2] Koshlak H., *Synthesis of Zeolites from Coal Fly Ash Using Alkaline Fusion and Its Applications in Removing Heavy Metals.* Materials (Basel). 2023 Jul 5; 16(13):4837. Doi: 10.3390/ma16134837. PMID: 37445151; PMCID: PMC10343740.

[3] Pleśniak J., Trzop W., *Codzienność z zeolitami.* Zeolites in everyday life; Analit 2 (2016), pp. 146-151; 1.

[4] Telka J.M., *Mezomikroporowate zeolity i zeotypy w aspekcie ich katalitycznych zastosowań w procesach transformacji węglowodorów i alkoholi*, Kraków 2018.

[5] Winczaszek B.A., *Analiza możliwości zastosowania zeolitów syntetycznych z popiołów lotnych w procesach oczyszczania ścieków*, Wrocław 2006.

[6] https://market.us/report/zeolite-market/ Access in day 16.07.2023.

[7] Narang K., *Tailoring of adsorptive properties of zeolites for Biogas Upgrading*. Engineering Materials Division of Materials Science Department of Engineering Sciences and Mathematics (TVM); Luleå 2019.

[8] Książek S., Kida M., Koszelnik P., *Możliwości katalitycznego zastosowania materiałów odpadowych*. Czasopismo Inżynierii Lądowej, Środowiska i Architektury Journal of Civil Engineering, Environment and Architecture Jceea, t. XXXIV, z. 64 (2/II/17), kwiecień-czerwiec 2017, s. 55-62, DOI: 10.7862/rb.2017.81.

[9] Koshlak H., *Improving the environmental safety of coal-fired thermal power plants by using fly ash in recycling technology*. Journal of New Technologies in Environmental Science, 2021, 4(2), pp. 135-142, jntes.tu.kielce.pl/wp-content/uploads/2022/02/IMPROVING-THE-ENVIRONMENTAL-SAFETY-OF-COAL-FIRED-THERMAL-POWER-PLANTS-BY-USING-FLY-ASH-IN-RECYCLING-TECHNOLOGY.pdf.

[10] Qazi U., Javaid R., Ikhlaq A., Khoja A., Saleem F., *A Comprehensive Review on Zeolite Chemistry for Catalytic Conversion of Biomass/Waste into Green Fuels*. Molecules 2022, 27(23), 8578, https://doi.org/10.3390/molecules27238578; https://www.mdpi.com/1420-3049/27/23/8578.

[11] Wdowin M., Baran P., Panek R., Zarębska K., Franus W., *Analiza możliwości oczyszczania gazów wylotowych z HgO i CO_2 na zeolitach syntetycznych otrzymanych z popiołów lotnych*, Volume/Tom 17. Year/Rok 2015 ISSN 1506-218X, s. 1306-1319.

[12] Shabani J., Ameh A., Oyekola O., Babajide O., Petrik L., *Fusion-Assisted Hydrothermal Synthesis and Post-Synthesis Modification of Mesoporous Hydroxy Sodalite Zeolite Prepared from Waste Coal Fly Ash for Biodiesel Production.* Catalysts 2022, 12(12), 1652, https://doi.org/10.3390/catal12121652; https://www.mdpi.com/2073-4344/12/12/1652.

[13] Gao Z., Xiang M., He M., Zhou W., Chen J., Lu J., Wu Z., Su Y., *Transformation of CO2 with Glycerol to Glycerol Carbonate over ETS-10 Zeolite-Based Catalyst.* Molecules 2023, 28(5), 2272, https://doi.org/10.3390/molecules28052272; https://www.mdpi.com/1420-3049/28/5/2272.

[14] Koshlak H., *Gas Formation Reactions in the Raw Mixture Based on TPP Ash.* Rocz. Ochr. Śr. 2021; 23:106-116. Doi: 10.54740/ros.2021.007.

[15] Gjyli S., Korpa A., Teneqja V., Siliqi D., Belviso C., *Siliceous Fly Ash Utilization Conditions for Zeolite Synthesis.* Environ. Sci. Proc. 2021, 6(1), 24, https://doi.org/10.3390/iecms2021-09359; https://www.mdpi.com/2673-4931/6/1/24.

[16] Oszust M., Barczak M., Dąbrowski A., *Mezoporowate materiały krzemionkowe – Charakterystyka i zastosowanie* [in] Nauka dla gospodarki 2/2012 Adsorbenty i katalizatory. Wybrane technologie a środowisko, Rzeszów 2012, s. 53-68.

[17] Łach M., Mierzwiński D., Mikuła J., *Synteza zeolitów z popiołów i żużli ze spalarni odpadów*, Inżynieria Ekologiczna Ecological Engineering Vol. 18, Iss. 1, Feb. 2017, pages 196-201. DOI: 10.12912/23920629/68199.

[18] Lulu Deng, Qiyong Xu, Huanan Wu, *Synthesis of zeolite-like material by hydrothermal and fusion methods using municipal solid waste fly ash*. Procedia Environmental Sciences 31 (2016) 662-667, 2016. Doi: 10.1016/j.proenv.2016.02.122.

[19] Al-Zeer M., MacKenzie K., *Fly Ash-Based Geopolymers as Sustainable Bifunctional Heterogeneous Catalysts and Their Reactivity in Friedel-Crafts Acylation Reactions.* Catalysts 2019, 9(4), 372, https://doi.org/10.3390/catal9040372; https://www.mdpi.com/2073-4344/9/4/372.

[20] Feng W., Lu X., Xiong J., Yu Z., Wang Y., Cui J., Zhang R., Weng R., *Solid–Waste–Derived Geopolymer–Type Zeolite–like High Functional Catalytic Materials Catalyze Efficient Hydrogenation of Levulinic Acid*. Catalysts 2022, 12(11), 1361, https://doi.org/10.3390/catal12111361; https://www.mdpi.com/2073-4344/12/11/1361.

[21] Soleymani Angili T., Grzesik K., Jerzak W., *Comparative Life Cycle Assessment of Catalytic Intermediate Pyrolysis of Rapeseed Meal.* Energies 2023, 16(4), 2004, https://doi.org/10.3390/en16042004; https://www.mdpi.com/1996-1073/16/4/2004.

[22] Kremer I., Tomić T., Katančić Z., Hrnjak-Murgić Z., Erceg M., Vecchio Ciprioti S., Schneider D., *Effect of Zeolite Catalyst on the Pyrolysis Kinetics of Multi-Layered Plastic Food Packaging.* Symmetry 2022, 14(7), 1362, https://doi.org/10.3390/sym14071362; https://www.mdpi.com/2073-8994/14/7/1362.

[23] Cocchi M., Angelis D., Mazzeo L., Nardozi P., Piemonte V., Tuffi R., Vecchio Ciprioti S., *Catalytic Pyrolysis of a Residual Plastic Waste Using Zeolites Produced by Coal Fly Ash.* Catalysts 2020, 10(10), 1113, https://doi.org/10.3390/catal10101113; https://www.mdpi.com/2073-4344/10/10/1113.

[24] Rodríguez-Iznaga I., Shelyapina M., Petranovskii V., *Ion Exchange in Natural Clinoptilolite: Aspects Related to Its Structure and Applications.* Minerals 2022, 12(12), 1628, https://doi.org/10.3390/min12121628; https://www.mdpi.com/2075-163X/12/12/1628.

[25] Hao Xu, Peng Wu, *New progress in zeolite synthesis and catalysis*. National Science Review 9: nwac045, 2022, https://doi.org/10.1093/nsr/nwac045.

[26] Cederick Cyril Amoo, Chuang Xing, Noritatsu Tsubaki, and Jian Sun, *Tandem Reactions over Zeolite-Based Catalysts in Syngas Conversion,* ACS Central Science 2022 8 (8), 1047-1062. DOI: 10.1021/acscentsci.2c00434.